Tail-GAN: Simulation of extreme events with ReLU neural networks

Michaël Allouche, Stéphane Girard, Emmanuel Gobet

Tail-GAN: Simulation of extreme events with ReLU neural networks

Michaël Allouche michael.allouche@polytechnique.edu
Centre de Mathématiques Appliquées (CMAP), CNRS, Ecole Polytechnique
Institut Polytechnique de Paris, Route de Saclay, 91128 Palaiseau Cedex, France

Stéphane Girard stephane.girard@inria.fr
Univ. Grenoble Alpes, Inria, CNRS, Grenoble INP, LJK
38000 Grenoble, France

Emmanuel Gobet emmanuel.gobet@polytechnique.edu
Centre de Mathématiques Appliquées (CMAP), CNRS, Ecole Polytechnique
Institut Polytechnique de Paris, Route de Saclay, 91128 Palaiseau Cedex, France

Abstract

Feedforward neural networks based on Rectified linear units (ReLU) cannot efficiently approximate quantile functions which are not bounded, especially in the case of heavy-tailed distributions. We thus propose a new parametrization for the generator of a Generative adversarial network (GAN) adapted to this framework, basing on extreme-value theory. We provide an analysis of the uniform error between the extreme quantile and its GAN approximation. It appears that the rate of convergence of the error is mainly driven by the second-order parameter of the data distribution. The above results are illustrated on simulated data and real financial data.

Keywords: Extreme Value Theory, neural networks, generative models
2020 MSC: 68T07, 60G70

1. Introduction

Context of risks. Analyzing extreme events is an important issue in economics, engineering, and life sciences, among other fields, with significant applications such as actuarial risks (Asmussen and Albrecher, 2010), communication network reliability (Robert, 2003), aircraft safety (Prandini and Watkins, 2005), analysis of epidemics, and so forth... In the last two decades, it has taken even more importance in financial risk management, because of the increasing number of shocks and financial crises. Among the wide range of exercises in this field, stress test (European Banking Authority, 2014) has become a main guideline for the regulator in order to assess the banking system resilience against the realizations of various categories of risk (market, credit, operational, climate, etc). To this end, numerical simulation of unfavorable extreme (but plausible) scenarios is a major tool to study the consequences on these risks. Given a stochastic model of risks, various sampling schemes are available (for instance, using importance sampling (Bucklew, 2004, Chapter 4), MCMC with splitting – (Gobet and Liu, 2015), or interacting particles system – (Del Moral and Garnier, 2005)), with the potential advantage of reducing the statistical fluctuation over a naive Monte Carlo method. Though presumably more informative for a given number M of samples, these methods suffer from a higher computational complexity (notably in high

dimension): Thus, one might wonder how to get extra samples in an efficient way, by leveraging the previous M samples. Somehow, the situation is similar to a case where the previous samples are viewed as observed data and where we seek a data-driven method able to sample similarly to that empirical distribution, without necessarily the knowledge of the sampling method that has generated the observed data. This corresponds to the recent paradigm of Generative adversarial network (GAN) models initiated by (Goodfellow et al., 2014) or of Variational autoencoder (VAE) by (Kingma and Welling, 2014). The novelty in our work is relative to the context of risks, where we are interested in a generative data-based model able to reproduce – with high-fidelity – specific extreme statistical properties, while being fast in the simulation phase. The issue is also meaningful out of the context of generating the learning data set by sophisticated Monte Carlo methods, *i.e.* when they correspond to true historical data, as if we were in a pure statistical modeling framework (see experiments in Section 3).

Background results. Generally speaking, different types of generative models have been developed lately (Foster, 2019) and in this work, we focus on GANs, which have gained a tremendous popularity from the original work of (Goodfellow et al., 2014) and its extension using the Wasserstein distance (Arjovsky et al., 2017). Kuratowski Theorem (Bertsekas and Shreve, 1978, Chapter 7)-(Villani, 2009, p.8) ensures that any random variable X on $\mathbb{R}^d$ (and more generally on a Polish space) can be obtained by

$$X \overset{d}{=} G(Z) \tag{1}$$

for some measurable function G and some latent random variable Z in dimension d' (see Lemma 7 in the Appendix for a constructive proof with $Z \sim \mathcal{U}([0,1])$ and $d' = 1$) such that for each mth marginal, $m \in \{1, \dots, d\}$, one has $\tilde{X}^{(m)} := G^{(m)}(Z) \overset{\mathrm{d}}{=} X^{(m)}$. This result is one key to understand the ability of GANs to simulate realistic samples in a space of high dimension d, starting from a latent space of moderate dimension d'. In practice, the selection of this latent dimension is an open problem in the generative neural networks literature. A GAN scheme is aimed at approximating the unknown G through a parametric family of Neural networks (NN) $\mathcal{G} = \{G_\theta : \mathbb{R}^{d'} \to \mathbb{R}^d, \theta \in \Theta\}$ and to learn the optimal parameter $\theta^\star$ from a data set $\{X_i \in \mathbb{R}^d, i = 1, \dots, n\}$ of i.i.d samples from an unknown distribution p_X. It is performed by optimizing an objective function which can be interpreted as an adversarial game between a generator and a discriminator chosen in a parametric family of functions $\mathcal{D} = \{D_\phi : \mathbb{R}^d \to [0,1], \phi \in \Phi\}$. In other words, $D_\phi(x)$ represents the probability that an observation x is drawn from p_X. Both the generator and the discriminator are neural networks with opposite objectives: The former tries to mimic real data which seem likely by the discriminator, while the latter tries to distinguish between the two sources. In (Goodfellow et al., 2014), this optimization problem is defined as:

$$\min_{\theta\in\Theta} \max_{\phi\in\Phi} \left[\mathbb{E}_{p_X}\left(\log D_\phi(X)\right) + \mathbb{E}_{p_Z}\left(\log\left(1 - D_\phi\left(G_\theta(Z)\right)\right)\right)\right].$$

See (Biau et al., 2020a,b; Haas and Richter, 2020) for theoretical results and (Wiese et al., 2020; Zhou et al., 2018; Remlinger et al., 2021) for the generation of financial time-series.

To the best of our knowledge, extreme events generation is only addressed by (Bhatia et al., 2020) where the authors proposed first a distribution shifting in order to reduce the

lack of training data in the extreme tails. Second, a GAN parametrization conditioned by samples drawn from a generalized Pareto distribution is fitted to the shifted data. Finally, an additional term representing some distance to a desired extremeness is added to the loss function. Although numerical results on images are promising, we do not think that the proposed parametrization gives theoretical support for generating extreme observations.

Our contributions. In a GAN setting, our purpose is to cope with two prominent issues, that are mostly related to extreme-value theory. First, the number of data available in extreme regions must be relatively small, by definition (even in the case of data that are output of sophisticated sampling methods). Second, we restrict to the challenging situation of heavy-tailed distributions (in the Fréchet maximum domain of attraction), where by definition, extreme data take very large values. Therefore, the usual GAN approach cannot work, as we now explain (and as the reader will check from our numerical experiments in Section 3). Consider for a while the case $d = d' = 1$ and say that G in (1) is approximated by a ReLU NN under the form

$$G_\theta(z) = \sum_{j=1}^{J} a_j \sigma(w_j z + b_j), \tag{2}$$

where $\sigma(x) := \max(x, 0)$ is the ReLU function, $\theta = \{(a_j, w_j, b_j),\, j = 1, \dots, J\} \in \Theta = \mathbb{R}^{3J}$ and J is the number of units in the hidden layer. On the one-hand, if the latent random variable Z were bounded, the output would be bounded and by no means, it would be a good candidate for fitting the distribution of the unbounded random variable X. On the other hand, taking for Z a Gaussian vector as it is often chosen, for example in (Bhatia et al., 2020), would lead to a light-tailed distribution for $G_\theta(Z)$ since G_θ is sublinear w.r.t. the input (Vladimirova et al., 2018), whereas we focus on the heavy-tail case. Clearly, such a parameterization (2) of the generator cannot be efficient when extreme values are concerned. Note that deeper NN would not overcome this issue either.

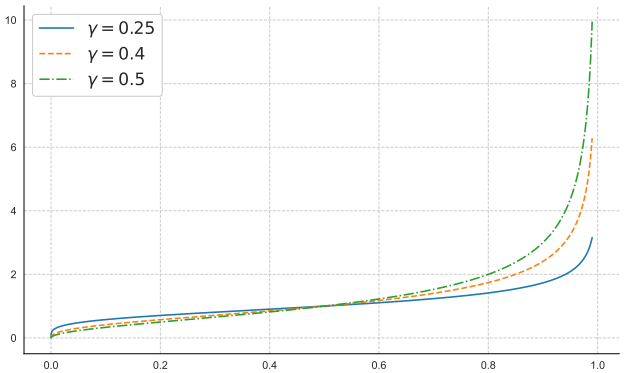

Figure 1: Quantile function associated with the Burr distribution $u \in (0, 1) \mapsto q_X(u)$ with tail-index $\gamma \in \{0.25, 0.4, 0.5\}$ and second-order parameter $\rho = -1$, see Table 4 for the parameterization.

To introduce our new parametrization (called Tail-GAN), consider X a real random variable with cumulative distribution function F_X defined on $\mathbb{R}$. The inversion method by Von Neumann Eckhardt (1987) gives that one can set $G(u) := q_X(u) := \inf\{x : F_X(x) \geq u\}$ with $U \sim \mathcal{U}([0,1])$. Since we shall focus on distributions in the Fréchet maximum domain of attraction (de Haan and Ferreira, 2006, Theorem 1.2.1) with positive tail-index γ, the associated survival function $\bar{F}_X(x) := 1 - F_X(x)$ decays at rate $x^{-1/\gamma}$ when $x \to \infty$, which implies that $q_X(u)$ diverges as $u \to 1$ at rate $(1-u)^{-\gamma}$. The tail-index γ is thus the main driver of the behavior of extreme quantiles, see Figure 1 for an illustration. To be in a position to apply results like the Universal approximation theorem (Cybenko, 1989) (any continuous function on $[0,1]$ can be approximated with arbitrary precision by a one hidden layer neural network), we shall transform the quantile function to avoid divergence in the neighborhood of $u = 1$. To this end, for all $(u, y) \in [0,1) \times (0, \infty)$, let

$$H_u(y) = -\log(y) \,/ (\log(1-u^2) - \log(2)) \qquad \text{and} \qquad f^{\mathrm{TIF}}(u) = H_u(q_X(u)). \tag{3}$$

It will appear in the sequel that f^{TIF} is continuous on $[0,1]$ for all F_X in the Fréchet maximum domain of attraction, with $f^{\mathrm{TIF}}(u) \to \gamma$ as $u \to 1$; f^{TIF} is thus referred to as the Tail-index function (TIF). Therefore, a ReLU NN could well approximate f^{TIF} thanks to the Universal approximation theorem, but to get even better approximation, we shall consider a correction of the Tail-index function:

$$f^{\mathrm{CTIF}}(u) = f^{\mathrm{TIF}}(u) - \sum_{k=1}^{6} \kappa_k e_k(u), \quad u \in [0,1],$$

which enjoys higher regularity in the neighborhood of $u = 1$. See Paragraph 2.2 for a definition of functions $e_1, \ldots, e_6$ and coefficients $\kappa_1, \ldots, \kappa_6$. Now use a NN to approximate the smooth function f^{CTIF}, deduce an approximation of f^{TIF}, and of the quantile function by composing with H_u^{-1} for each u (in view of (3)): all in all, we obtain the so-called tail-GAN parametrization defined for all $(z, x) \in [0,1] \times (0, \infty)$ as

$$G_\psi^{\mathrm{TIF}}(z) = H_z^{-1}\left(\sum_{j=1}^{J} a_j \sigma(w_j z + b_j) + \sum_{k=1}^{6} \kappa_k e_k(z)\right), \tag{4}$$

$$\text{with} \qquad H_z^{-1}(x) := \left(\frac{1-z^2}{2}\right)^{-x}. \tag{5}$$

In the multidimensional setting $d > 1$ and $d' > 1$, our strategy of approximation consists in preserving the same parametric form for each marginal component, and in mixing the latent components to generate dependence between the d coordinates (see Corollary 6): the m-th coordinate will take the form, with $z = (z^{(1)}, \ldots, z^{(d)})$,

$$G_\psi^{\mathrm{TIF}(m)}(z^{(1)}, \ldots, z^{(d')}) = H_{z^{(m)}}^{-1}\left(\sum_{j=1}^{J} a_j^{(m)} \sigma\left(\sum_{i=1}^{d'} w_j^{(i)} z^{(i)} + b_j\right) + \sum_{k=1}^{6} \kappa_k^{(m)} e_k\left(z^{(m)}\right)\right). \tag{6}$$

Let us highlight that, in (6), the mth coordinate of the generator $G_\psi^{\mathrm{TIF}}(z)$ involves the mth coordinate of z which is a $d'-$ dimensional vector. The above construction of the tail-GAN

generator thus constraints the latent dimension to be larger than the dimension of the data: $d' \geq d$. The architecture of the associated neural network is illustrated on Figure 2 in the case $d = 2$ and $d' = 3$.

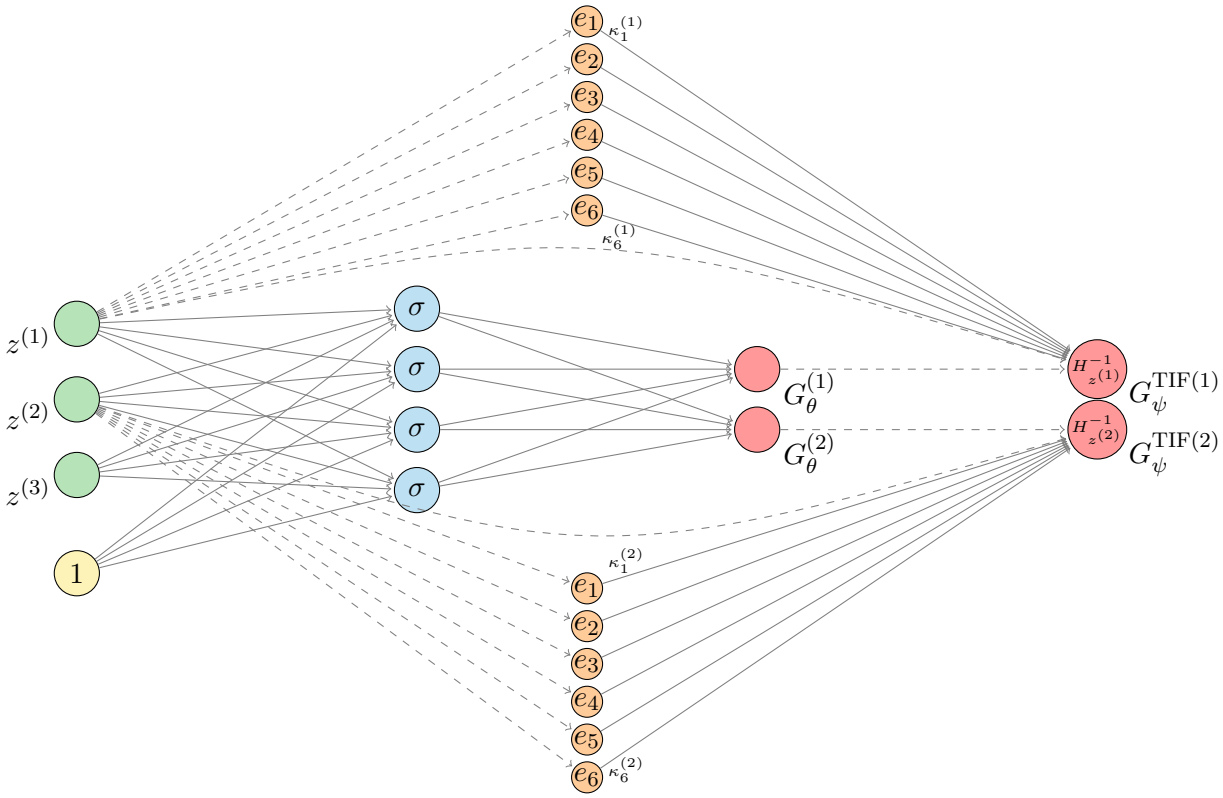

Figure 2: Generator of the Tail-GAN with one hidden layer, $d' = 3$ and $d = 2$.

We prove in Theorem 5 that the above tail-GAN parametrization converges uniformly coordinate-wise, in the log-scale of the $H_\cdot$-transform. Joint convergence for all coordinates is an open question, which is related to the delicate notion of upper tail dependence. However, numerical experiments in multidimensional setting fully support the relevance of this parametrization. We observe that tail dependencies are extremely well reproduced.

The rest of the paper is organized as follows. The transformation of the quantile function q_X associated with an heavy-tailed distribution F_X into a regular function f^{CTIF} is presented in Section 2: Under a second-order assumption, we show that f^{CTIF} can be uniformly approximated by a one-hidden layer neural network with some rate depending on the second-order parameter ρ. Auxiliary results and technical proofs are postponed to Appendix. The

performance of the method is illustrated on simulated data (Section 3) and real financial data (Section 4). It is shown that, in both experiments, our approach largely outperforms the classic GAN method. Some conclusions and directions of future research are discussed in Section 5.

2. Main results

First, the construction of the proposed transformation of the quantile function is developed and its approximation by a ReLU NN is then investigated.

2.1 TIF regularity

In this section, we discuss the construction and the extension of (3). The objective is to build a tail-index function which may be well approximated by a neural network. Let X be a real random variable and denote by F_X its cumulative distribution function supposed to be continuous and strictly increasing. We focus on the case of heavy-tailed distributions, *i.e.* when F_X is attracted to the maximum domain of Pareto-type distributions with tail-index $\gamma > 0$. From Bingham et al. (1987), the survival function $\bar{F}_X := 1 - F_X$ of such a heavy-tailed distribution can be expressed as

($\mathbf{H_1}$): $\bar{F}_X(x) = x^{-1/\gamma}\ell_X(x)$, where ℓ_X is a slowly-varying function at infinity *i.e.* such that $\ell_X(\lambda x)/\ell_X(x) \to 1$ as $x \to \infty$ for all $\lambda > 0$.

In such a case, $\bar{F}_X$ is said to be regularly-varying with index $-1/\gamma$ at infinity, which is denoted for short by $\bar{F}_X \in RV_{-1/\gamma}$. The tail-index γ tunes the tail heaviness of the distribution function F_X. Assumption ($\mathbf{H_1}$) is recurrent in risk assessment, since actuarial and financial data are most of the time heavy-tailed, see for instance the recent studies Alm (2016); Chavez-Demoulin et al. (2014) or the monographs Embrechts et al. (1997); Resnick (2007). As a consequence of the above assumptions, the tail quantile function $x \mapsto q_X(1 - 1/x)$ is regularly-varying with index γ at infinity, see (de Haan and Ferreira, 2006, Proposition B.1.9.9), or, equivalently,

$$q_X(u) = (1-u)^{-\gamma} L\left(\frac{1}{1-u}\right), \tag{7}$$

for all $u \in (0,1)$ with L a slowly-varying function at infinity. Without of loss of generality, one can assume that $\eta := \mathbb{P}(X \geq 1) \neq 0$ and, since, we focus on the upper tail behavior of X, introduce the random variable $Y = X$ given $X \geq 1$. It follows that quantile function of Y is given by

$$q_Y(u) = q_X(1 - (1-u)\eta), \tag{8}$$

for all $u \in (0,1)$. Finally, we consider the Tail-index function (TIF) obtained by plugging (8) into (3):

$$f^{\mathrm{TIF}}(u) = -\frac{\log q_X\big(1-(1-u)\eta\big)}{\log(1-u^2) - \log 2}, \tag{9}$$

for all $u \in (0,1)$. The next Proposition provides some preliminary properties of the above TIF, see Figure 3 for an illustration on the Burr distribution defined in Table 4.

Proposition 1 *Under* $(\mathbf{H_1})$, f^{TIF} *is a continuous and bounded function on* $[0,1]$. *Besides,* $f^{\mathrm{TIF}}(0) = 0$ *and* $f^{\mathrm{TIF}}(u) \to \gamma$ *as* $u \to 1$.

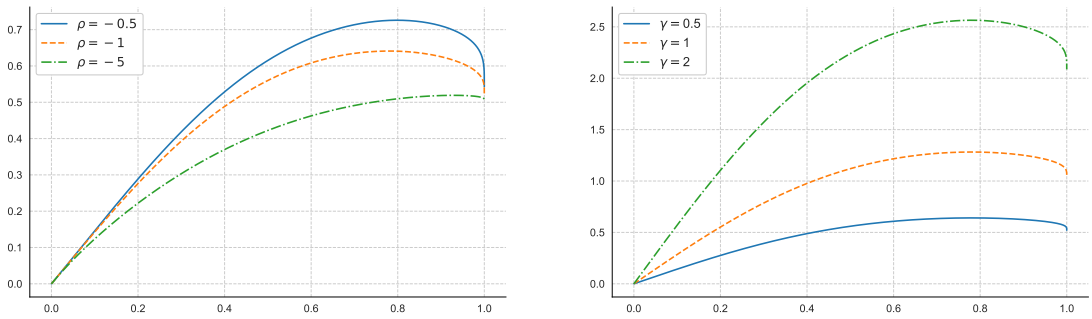

(a) $\gamma = 1/2$ and $\rho \in \{-5, -1, -1/2\}$ (b) $\rho = -1$ and $\gamma \in \{1/2, 1, 2\}$

Figure 3: Tail-index function $u \in (0,1) \mapsto f^{\mathrm{TIF}}(u)$ associated with Burr distribution for different values of tail-index γ and second-order parameter ρ, see Table 4 for parameterization details.

In contrast to the quantile function, the TIF is bounded on $[0,1]$. We now focus on the behavior of the first derivative of the TIF, which will appear to depend on an additional tail parameter ρ, as it may be guessed from Figure 3. Extra assumptions on F_X, or equivalently on L, are necessary such that f^{TIF} is differentiable. Consider the Karamata representation of the slowly-varying function L (de Haan and Ferreira, 2006, Definition B1.6):

$$L(x) = c(x) \exp\left(\int_1^x \frac{\varepsilon(t)}{t}\,\mathrm{d}t\right), \tag{10}$$

where $c(x) \to c_\infty$ as $x \to \infty$ and ε is a measurable function such that $\varepsilon(x) \to 0$ as $x \to \infty$. Our second main assumption then writes:

$(\mathbf{H_2})$: $c(x) = c_\infty > 0$ for all $x \geq 1$ and $\varepsilon(x) = x^\rho \ell(x)$ with $\ell \in RV_0$ and $\rho < 0$.

The assumption that c is a constant function is equivalent to assuming that L is normalized (Kohlbecker, 1958) and ensures that L is differentiable. As noted in Bingham et al. (1987), the normalization assumption is not restrictive since slowly-varying functions are of interest only to within asymptotic equivalence. The condition $\varepsilon \in RV_\rho$ with $\rho < 0$ entails that $L(x) \to L_\infty \in (0, \infty)$ as $x \to \infty$. The index of regular variation ρ is referred to as the second-order parameter. It is the main driver of the bias in the estimation of extreme quantiles from heavy-tailed distributions, see Table 4 for values of ρ associated with usual distributions. Besides, $(\mathbf{H_2})$ entails that F_X satisfies the so-called second-order condition which is the cornerstone of all proofs of asymptotic normality in extreme-value statistics. Interpretations and examples may be found in Beirlant et al. (2004) and de Haan and Ferreira (2006). We also refer to Gardes and Girard (2010, 2012) where a similar assumption is introduced in the framework of conditional extremes. Similarly, we shall also consider the assumption:

($\mathbf{H_3}$): ℓ is normalized.

The latter condition ensures that ℓ is differentiable on $(0,1)$ and thus that L and q_X are twice differentiable on $(0,1)$. Our second result provides a precise expansion of the first order derivative of f^{TIF} in the neighborhood of 1.

Proposition 2 *Assume* ($\mathbf{H_1}$) *and* ($\mathbf{H_2}$) *hold. Then,* f^{TIF} *is continuously differentiable on* $(0,1)$ *and*

$$\partial_u f^{\mathrm{TIF}}(0) = \frac{\gamma + \varepsilon\left(1/\eta\right)}{\log(2)},$$

$$\partial_u f^{\mathrm{TIF}}(u) = \sum_{j=0}^{3} c_j \varphi_j(u) - \frac{\varepsilon\left(\frac{1}{(1-u)\eta}\right)}{(1-u)\log(1-u)}\left(1+o(1)\right) + \mathcal{O}\left(\frac{(1-u)}{\log(1-u)}\right), \tag{11}$$

as $u \to 1$, *where* $c_0 = c_3 = \beta$, $c_1 = -\gamma/2$, $c_2 = (\gamma-\beta)/2$, $\beta = \gamma\log\eta - \log L_\infty$,

$$\varphi_0(u) = \frac{1}{(1-u)\left(\log(1-u)\right)^2} \text{ and } \varphi_j(u) = \frac{1}{\left(\log(1-u)\right)^j},\ u \in (0,1),\ j = 1,2,3.$$

Let us highlight that $\varphi_0(u) \to \infty$ as $u \to 1$ making the first derivative of f^{TIF} unbounded as $u \to 1$, see Figure 4a for an illustration on the Burr distribution. In contrast, $\varphi_j(u) \to 0$ as $u \to 1$ for all $j \in \{1,2,3\}$ while the second term in (11) tends to 0 if $\rho < -1$ or tends to ∞ if $\rho > -1$. Moreover, it is readily seen that $\partial_u \varphi_j(u) \to \infty$ as $u \to 1$ for all $j \in \{0,\ldots,3\}$. As a conclusion, in the case where $\rho < -1$, it is possible to build a twice differentiable version of f^{TIF} by removing the φ_j components, $j \in \{0,\ldots,3\}$, in the neighborhood of $u = 1$. To this end, consider

$$f^{\mathrm{CTIF}}(u) := f^{\mathrm{TIF}}(u) - g(u)\sum_{j=0}^{3} c_j \Phi_j(u) - \gamma g(u) - \partial_u f^{\mathrm{TIF}}(0) h(u), \tag{12}$$

with, for all $u \in (0,1)$,

$$\begin{aligned}
g(u) &= -4u^5 + 5u^4,\\
h(u) &= u^3 - 2u^2 + u,\\
\Phi_0(u) &= \varphi_1(u),\\
\Phi_1(u) &= -\operatorname{li}(1-u),\\
\Phi_2(u) &= \Phi_1(u) + (1-u)\varphi_1(u),\\
\Phi_3(u) &= \Big(\Phi_1(u) + (1-u)(\varphi_1(u) + \varphi_2(u))\Big)/2.
\end{aligned}$$

Here, $\operatorname{li}(\cdot)$ denotes the logarithmic integral function defined as $\operatorname{li}(x) := \int_0^x \frac{1}{\log(t)}\,\mathrm{d}t$ for all $0 < x < 1$, with $\operatorname{li}(0) = 0$ and $\operatorname{li}(x) \to -\infty$ as $x \to 1$. Let us remark that $g(\cdot)$ and $h(\cdot)$ are two Hermite spline functions and that, by construction, $\partial_u \Phi_j(u) = \varphi_j(u)$, for all $j \in \{0,\ldots,3\}$. The second term in (12) thus aims at removing the singular components in the first and second derivative of the TIF function in the neighborhood of $u = 1$. The additional terms $\gamma g(u)$ and $\partial f^{\mathrm{TIF}}(0) h(u)$ ensure that the TIF function as well as its first derivative vanish at $u = 0$. Regularity properties of f^{CTIF} are established in the next Proposition and illustrated on Figure 4 in the case of a Burr distribution.

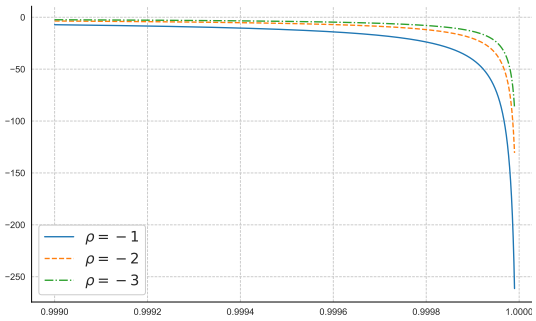

(a) TIF with $\gamma = 1/2$ and $\rho \in \{-3, -2, -1\}$

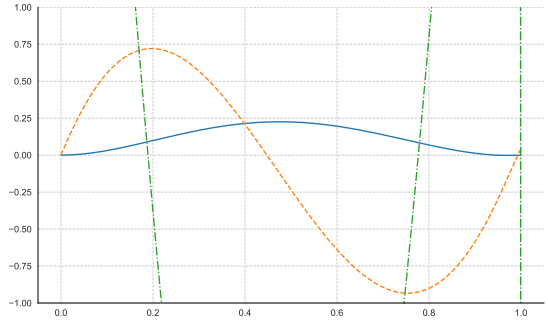

(b) CTIF with $\gamma = 1/2$ and $\rho = -1$

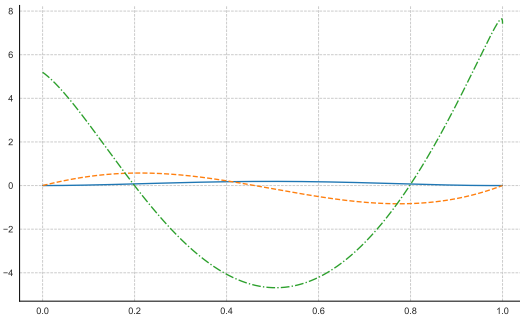

(c) CTIF with $\gamma = 1/2$ and $\rho = -2$

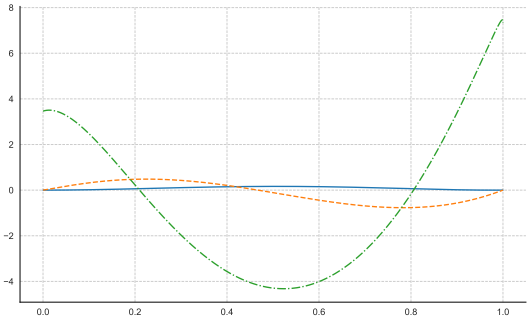

(d) CTIF with $\gamma = 1/2$ and $\rho = -3$

Figure 4: Illustration of the regularity properties of TIF and CTIF on a Burr distribution with $\gamma = 1/2$ and $\rho \in \{-3, -2, -1\}$. (a): First derivative of Tail index function $\partial_u f^{\text{TIF}}$. (b),(c),(d): Corrected tail-index function f^{CTIF} (solid blue line) and its first two derivatives $\partial_u f^{\text{CTIF}}$ (dashed orange line) and $\partial^2_{uu} f^{\text{CTIF}}$ (dash-dot green line).

Proposition 3

(i) If $(\mathbf{H_1})$ *holds, then*

$$\lim_{u \to 0} f^{\text{CTIF}}(u) = \lim_{u \to 1} f^{\text{CTIF}}(u) = 0. \tag{13}$$

(ii) If, moreover, $(\mathbf{H_2})$ *holds with* $\rho < -1$*, then* f^{CTIF} *is continuously differentiable on* $[0, 1]$ *and*

$$\lim_{u \to 0} \partial_u f^{\text{CTIF}}(u) = \lim_{u \to 1} \partial_u f^{\text{CTIF}}(u) = 0. \tag{14}$$

(iii) If, moreover, $(\mathbf{H_3})$ *holds, then* f^{CTIF} *is twice continuously differentiable on* $[0, 1)$ *and*

$$\partial^2_{uu} f^{\text{CTIF}}(u) = 20\gamma - 2\left(\frac{\gamma + \varepsilon(1/\eta)}{\log(2)}\right) - \frac{(1+\rho)\varepsilon\left(\frac{1}{\eta(1-u)}\right)}{(1-u)^2 \log(1-u)}(1 + o(1)) + \mathcal{O}\left(\frac{1}{\log(1-u)}\right), \tag{15}$$

as $u \to 1$ *and*

$$\lim_{u\to 0} \partial^2_{uu} f^{\mathrm{CTIF}}(u) = \frac{5\gamma + \varepsilon(1/\eta)\left(5 + \rho + \frac{1}{\eta}\frac{\partial \ell(1/\eta)}{\ell(1/\eta)}\right)}{\log(2)} - 5\beta. \tag{16}$$

(iv) If, moreover, $\rho < -2$*, then* f^{CTIF} *is twice continuously differentiable on* $[0,1]$ *and*

$$\lim_{u\to 1} \partial^2_{uu} f^{\mathrm{CTIF}}(u) = 20\gamma - 2\left(\frac{\gamma + \varepsilon(1/\eta)}{\log(2)}\right). \tag{17}$$

It appears on Figure 4b that for $\rho = -1$, property (13) holds while first and second derivatives do not vanish at the boundaries of $[0,1]$. When $\rho = -2$ (Figure 4c) both properties (13) and (14) are satisfied while the second derivative converges to a finite value in the neighborhood of 0, see (16), and diverges in the neighborhood of 1, see (15). Finally, $\rho = -3$ (Figure 4d) corresponds to the same situation, except that the second derivative also converges in the neighborhood of 1, see (17).

Let $I \subset \mathbb{R}$. Let us recall that a function $f : I \mapsto \mathbb{R}$ is Hölder continous with exponent $\alpha \in (0,1]$ if the following quantity is finite

$$[f]_\alpha := \sup_{x\neq y\in I} \frac{|f(x) - f(y)|}{|x-y|^\alpha}.$$

This property is denoted for short by $f \in H^\alpha(I)$. The case $\alpha = 1$ corresponds to Lipschitz functions. We shall also note $C^m(I)$ the set of m-th continuously differentiable functions on I, $m \in \mathbb{N}$. Finally, for all $\alpha \in (0,1]$ and $m \in \mathbb{N}$, we denote by $\mathcal{C}^{m,\alpha}(I)$ the Hölder space which consists of all functions $f \in C^m(I)$ such that $\partial^m f \in H^\alpha(I)$. In particular $\mathcal{C}^{m,1}(I) \subset \mathcal{C}^{m+1}(I)$. Using these notations, and focusing on the case where $\rho < -1$, the regularity properties of f^{CTIF} provided by Proposition 3 can be simplified as:

Corollary 4 *Assume* $(\mathbf{H_1})$*,* $(\mathbf{H_2})$ *and* $(\mathbf{H_3})$ *hold.*

(i) If $-2 \le \rho < -1$ *then* $f^{\mathrm{CTIF}} \in \mathcal{C}^{1,\alpha}([0,1))$ *for all* $\alpha \in (0, -1-\rho)$*.*

(ii) If $\rho < -2$ *then* $f^{\mathrm{CTIF}} \in C^2([0,1])$*.*

Let us note that higher regularities could be obtained at the price of further restrictions on ρ. We are now in a position to investigate how a neural network can approximate such a function.

2.2 Approximation error

Combining Corollary 4 and Lemma 13 in Appendix B provides the uniform approximation error of f^{CTIF} by a neural network depending on the number of ReLU functions:

Theorem 5 *Assume* $(\mathbf{H_1})$*,* $(\mathbf{H_2})$ *and* $(\mathbf{H_3})$ *hold. Let* σ *be a ReLU function. For all* $J \ge 6$*, there exist* $(a_j, w_j, b_j) \in \mathbb{R}^3$*,* $j = 1, \dots, J$ *such that:*

$$\sup_{u\in[0,1]} \left| f^{\mathrm{CTIF}}(u) - \sum_{j=1}^{J} a_j \sigma\left(w_j u + b_j\right) \right| \le \frac{[\partial_t f^{\mathrm{CTIF}}]_\alpha}{4} \left\lceil \frac{J-3}{3} \right\rceil^{-\alpha-1} = \mathcal{O}\left(J^{-\alpha-1}\right)$$

where

1. $\alpha \in (0, -1-\rho)$ *if* $-2 \leq \rho < -1$,
2. $\alpha = 1$ *if* $\rho < -2$.

In view of (12), letting $e_1(u) = g(u)$, $e_2(u) = h(u)$ and $e_{k+3}(u) = g(u)\Phi_k(u)$ for $k = 0, \ldots, 3$ in (4), the above approximation bounds on f^{CTIF} can be translated in terms of approximation bounds on f^{TIF} using the "enriched" neural network. Moreover, it can be done for all components of a d-dimensional random variable, by following the principle (6), with a latent dimension $d' \geq d$. We obtain the final approximation result which proof is now an easy combination of previous results.

Corollary 6 *Let σ be a ReLU function. Assume that $X = (X^{(1)}, \ldots, X^{(d)})^\top$ is a d-dimensional vector, which each component $X^{(m)}$ fulfilling $(\mathbf{H_1})$, $(\mathbf{H_2})$ and $(\mathbf{H_3})$ with some parameters $(\gamma^{(m)}, \rho^{(m)})$. Let $\mathcal{G}_J$ be the approximation space of TIF functions made of J neurons ($J \geq 6$):*

$$\mathcal{G}_J := \Bigg\{ G : z \in [0,1]^{d'} \mapsto G(z) = (G^{(1)}(z), \ldots, G^{(d')}(z))^\top,$$
$$G^{(m)}(z) = \sum_{j=1}^{J} a_j^{(m)} \sigma\left(\sum_{i=1}^{d'} w_j^{(i)} z^{(i)} + b_j \right) + \sum_{k=1}^{6} \kappa_k^{(m)} e_k\left(z^{(m)}\right),$$
$$a_j^{(m)}, w_j^{(i)}, b_j, \kappa_k^{(m)} \in \mathbb{R} \Bigg\}.$$

Then

$$\inf_{G \in \mathcal{G}_J} \sup_{m=1,\ldots,d} \sup_{z \in [0,1]^{d'}} \left| f^{\mathrm{TIF},(m)}(z^{(m)}) - G^{(m)}(z) \right| = \mathcal{O}\left(J^{-\alpha-1}\right)$$

where

(i) $\alpha \in (0, -1 - \max_{m=1,\ldots,d} \rho^{(m)})$ *if* $-2 \leq \rho^{(m)} < -1$ *for some* $m = 1, \ldots, d$,

(ii) $\alpha = 1$ *if* $\rho^{(m)} < -2$ *for all* $m = 1, \ldots, d$.

Here we have written

$$f^{\mathrm{TIF},(m)}(z^{(m)}) = -\frac{\log(q_{X^{(m)}}(1 - (1 - z^{(m)})\eta^{(m)}))}{\log\left(1 - \left(z^{(m)}\right)^2\right) - \log 2}$$

as an natural extension of (9). For optimal parameters $a_j^{(m)}, w_j^{(i)}, b_j, \kappa_k^{(m)}$, the generative model for X is then

$$\tilde{X} = H^{-1}_{Z^{(m)}}\left(G^{(m)}(Z)\right), \qquad Z \overset{\mathrm{d}}{=} \mathcal{U}([0,1]^{d'}) \tag{18}$$

where $H_u^{-1}(\cdot)$ is defined in (5).

In the above, one could restrict $G^{(m)}(z)$ to depend only on the m-th coordinate of z: it would not affect the potential quality of approximation of the m-th marginal of X but

it would lead to a generative model with independent components which is too restrictive. Mixing all latent components of z in $G^{(m)}(z)$ allows for generating dependence in the tails, while ensuring good fit of the marginals, as it will be checked in the subsequent experiments.

Observe that the worst[1] second-order parameter $\rho^{(m)}$ will tune the global accuracy of the Tail-GAN through the convergence order α.

3. Validation on simulated data

3.1 Experimental design

The simulation of our synthetic data is based on the use of copulas, which allow to model separately the dependence structure and the margins, see Appendix A for a short overview. We focus on the Gumbel copula, denoted by C_μ^G which has been proved to be the only max-stable Archimedean copula (Genest and Rivest, 1989). The associated generating function is $\psi_\mu^G(t) = \exp(-t^{1/\mu})$ defined for all $\mu \geq 1$ and $t \geq 0$. It is easily seen that Kendall's dependence function is given by $K_{C_\mu^G}(t) = t - t\log(t)/\mu$ for all $t \in (0, 1]$ and Kendall's tau is $\tau_{C_\mu^G} = 1 - 1/\mu$. These two above quantities respectively provide a local and global characterization of the dependence structure induced by the copula. Besides, $C_1^G = \Pi$ the independence copula, and $C_\mu^G \to M$, the comotonic copula, as $\mu \to \infty$. In our experiments, three values of the dependence parameter are investigated: $\mu \in \{1.1, 2, 10\}$ leading to $\tau_{C_\mu^G} \in \{0.1, 0.5, 0.9\}$. In the remaining part of this section, we restrict ourselves to the dimension $d = 2$, see Section 4 for illustrations in higher dimensions. The two margins are chosen to be Burr distributed, with common tail-index $\gamma := \gamma_1 = \gamma_2 \in \{0.1, 0.5, 0.9\}$ and second-order parameters $(\rho_1, \rho_2) \in \{(-1, -2), (-1, -3), (-2, -3)\}$, see Table 4 for the parametrization of the Burr distribution. Finally, $n = 10,000$ data $\{X_1, \ldots, X_n\}$ are simulated from the resulting bivariate model for the above $3 \times 3 \times 3 = 27$ combinations of parameters. In the sequel, we will denote by $\{\tilde{X}_1, \ldots, \tilde{X}_n\}$ the outputs generated either by the Tail-GAN model (18) or by the classic GAN.

The ranges of hyperparameters that we explored in order to find the best model for each data configuration are reported in Table 1. Note that in order to respect the architecture (6), the generator has been restricted to be a 1-hidden layer neural network. Additionally, we used the optimizer Adam (Kingma and Ba, 2014) with default parameters $\beta_1 = 0.9$ and $\beta_2 = 0.999$ for all tests performed during $1,000$ *epochs* (*i.e.* iterations).

3.2 Performance assessment

Recall that from (7), in the heavy-tail model, for all $j \in \{1, \ldots, d\}$, $\log q_{X^{(j)}}(u)$ is approximatively proportional to $\log(1/(1-u))$ when u is close to 1, with the tail-index γ as proportionality factor. It is therefore common practice to check the heavy-tail assumption on each margin $j \in \{1, \ldots, d\}$ by drawing a log quantile-quantile plot, namely the points $(\log((n+1)/i), \log X^{(j)}_{n-i+1,n})$, for $i \in \{1, \ldots, \lceil(1-\xi)n\rceil\}$, where $\xi \in [0, 1)$ is a given probability level. The performance of a generator can then be visually assessed by comparing the pairs $(\log((n+1)/i), \log X^{(j)}_{n-i+1,n})$ and $(\log((n+1)/i), \log \tilde{X}^{(j)}_{n-i+1,n})$. To further quantify the fit on the tails of the marginal distributions, we define the Sum squared logarithmic

1. the closest to -1

Hyperparameters ranges								
	latent dimension	batch size	neurons G.	learning rate G.	hidden layers D.	neurons D.	learning rate D.	training loop D.
	$[10, 100]$	$[5-64]$	$[10, 500]$	$[0.0001, 0.01]$	$[1, 4]$	$[10, 500]$	$[0.0001, 0.01]$	$[1, 5]$
Selected hyperparameters on simulated data								
	latent dimension	batch size	neurons G.	learning rate G.	hidden layers D.	neurons D.	learning rate D.	training loop D.
Tail-GAN	36 (13)	31 (18)	68 (54)	0.0004 (0.0004)	2 (0)	45 (39)	0.0004 (0.0004)	1 (0)
GAN	33 (12)	26 (16)	56 (30)	0.001 (0.0004)	2 (0)	42 (38)	0.001 (0.0004)	1 (0)
Selected hyperparameters on real data								
	latent dimension	batch size	neurons G.	learning rate G.	hidden layers D.	neurons D.	learning rate D.	training loop D.
Tail-GAN	21 (9)	11 (9)	17 (9)	0.0004 (0.0004)	3 (0)	13 (4)	0.0006 (0.0004)	1 (0)
GAN	49 (33)	10 (4)	77 (78)	0.0001 (0)	2 (1)	64 (86)	0.0006 (0.0004)	1 (1)

Table 1: Top: Hyperparameters ranges used for tuning GANs across the experiments. Center: Mean (standard deviation) of selected hyperpameters on simulated data according to the SSLE(0.99) and AKE criteria. Bottom: Mean (standard deviation) of selected hyperpameters on real data according to the SSLE(0.95) and AKE criteria.

error (SSLE) as the squared distance between the logarithm of the original and generated data:

$$\mathrm{SSLE}(\xi) = \frac{1}{d}\sum_{j=1}^{d}\sum_{i=1}^{\lceil(1-\xi)n\rceil}\left(\log(X^{(j)}_{n-i+1,n}) - \log(\tilde{X}^{(j)}_{n-i+1,n})\right)^2.$$

In the sequel, we consider $\xi \in \{0.90, 0.95, 0.99\}$. Considering the dependence structure, one may also graphically compare the estimated Kendall's dependence functions K (or equivalently the $t \mapsto \lambda(t) := t - K(t)$ functions) associated with the original sample and the generated one. From the quantitative point of view, the fit of the dependence structure is assessed by the 1-Wasserstein distance between these two Kendall's dependence functions which indeed are cumulative distribution functions. The distance can be computed as a L^1 norm referred to as the Absolute Kendall error (AKE) in the sequel:

$$\mathrm{AKE} = \frac{1}{n}\sum_{i=1}^{n}\left|Z_{i,n} - \tilde{Z}_{i,n}\right|,$$

where $Z_{1,n} \leq \cdots \leq Z_{n,n}$ (resp. $\tilde{Z}_{1,n} \leq \cdots \leq \tilde{Z}_{n,n}$) are the order statistics associated with $\{Z_1, \ldots, Z_n\}$ (resp. $\{\tilde{Z}_1, \ldots, \tilde{Z}_n\}$) and the $\tilde{Z}_i$ are computed similarly to (19) in Appendix A on the generated sample. We shall also compare Kendall's tau estimated on the original sample $\hat{\tau}_n$, on the generated sample $\tilde{\tau}_n$ and the theoretical value $\tau_{C^G_\mu}$.

3.3 Computational aspects

The numerical experiments presented in the next two sections have been conducted on the Cholesky computing cluster from Ecole Polytechnique `http://meso-ipp.gitlab.labos.`

SSLE(0.99)

γ	(ρ_1, ρ_2) \ μ	1.1		2		10	
0.1	$(-1,-2)$	0.895	**0.116**	0.545	**0.097**	0.232	**0.037**
	$(-1,-3)$	0.923	**0.103**	0.732	**0.082**	0.553	**0.143**
	$(-2,-3)$	0.677	**0.190**	0.836	**0.083**	0.700	**0.174**
0.5	$(-1,-2)$	3.576	**1.058**	10.673	**1.006**	2.567	**1.321**
	$(-1,-3)$	1.943	**0.958**	6.913	**1.569**	3.812	**3.252**
	$(-2,-3)$	10.809	**1.707**	10.157	**1.201**	1.306	**1.195**
0.9	$(-1,-2)$	47.742	**4.966**	55.360	**6.473**	57.186	**8.651**
	$(-1,-3)$	44.949	**3.129**	51.294	**4.573**	45.900	**3.205**
	$(-2,-3)$	68.438	**3.860**	36.304	**6.390**	44.814	**5.922**

AKE

γ	(ρ_1, ρ_2) \ μ	1.1		2		10	
0.1	$(-1,-2)$	3.122	**2.865**	7.385	**8.322**	2.807	**2.855**
	$(-1,-3)$	3.102	**2.293**	5.671	**6.958**	1.585	**2.415**
	$(-2,-3)$	2.519	**3.244**	4.596	**7.125**	1.823	**2.340**
0.5	$(-1,-2)$	3.052	**2.234**	4.857	**1.772**	2.265	**2.015**
	$(-1,-3)$	6.261	**2.342**	4.538	**1.665**	2.616	**1.301**
	$(-2,-3)$	5.772	**2.134**	12.277	**1.408**	4.245	**1.922**
0.9	$(-1,-2)$	2.555	**2.103**	5.030	**1.990**	2.567	**1.932**
	$(-1,-3)$	3.788	**1.861**	8.034	**1.700**	1.623	**1.429**
	$(-2,-3)$	3.611	**1.696**	5.632	**1.788**	1.991	**1.181**

Kendall's tau

γ	(ρ_1, ρ_2) \ μ ($\tau_{C_\mu^\theta}$)	1.1 (0.1)		2 (0.5)		10 (0.9)	
0.1	$(-1,-2)$	0.092	**0.091**	0.514	**0.531**	0.905	**0.895**
	$(-1,-3)$	0.093	**0.083**	0.477	**0.500**	0.900	**0.905**
	$(-2,-3)$	0.086	**0.083**	0.511	**0.480**	0.899	**0.903**
0.5	$(-1,-2)$	0.090	**0.088**	0.493	**0.500**	0.903	**0.900**
	$(-1,-3)$	0.106	**0.096**	0.506	**0.502**	0.901	**0.900**
	$(-2,-3)$	0.093	**0.087**	0.473	**0.502**	0.885	**0.898**
0.9	$(-1,-2)$	0.088	**0.090**	0.500	**0.503**	0.903	**0.901**
	$(-1,-3)$	0.091	**0.088**	0.484	**0.499**	0.899	**0.897**
	$(-2,-3)$	0.073	**0.089**	0.487	**0.498**	0.900	**0.900**

Table 2: Comparison between the best GAN and Tail-GAN (in bold) results on simulated data for the 27 combinations of parameters. Top: SSLE criterion at level $\xi = 0.99$, center: AKE criterion (the results are scaled by 10^3 for the sake of readability), bottom: Kendall's tau (using the same models as the ones based on the AKE criterion).

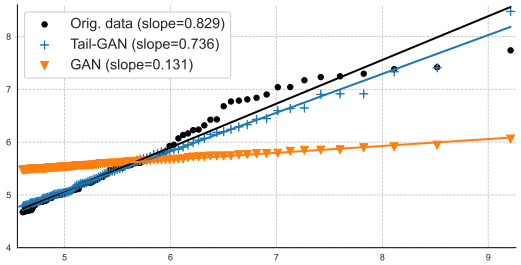

(a) First margin ($\gamma = 0.9, \rho_1 = -1$)

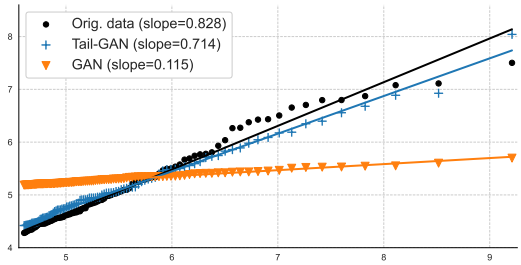

(b) Second margin ($\gamma = 0.9, \rho_2 = -3$)

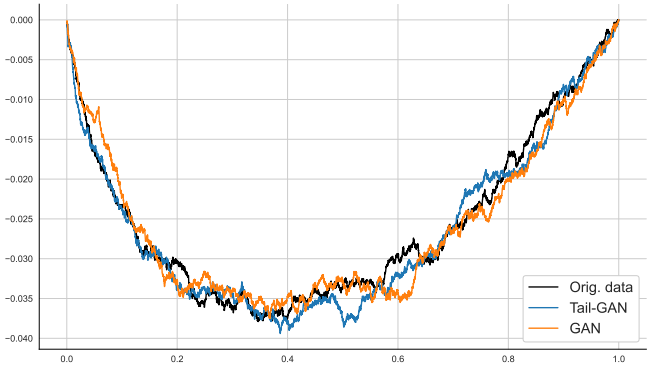

(c) Estimated $\lambda(\cdot)$ functions

Figure 5: Top: log quantile-quantile plots on simulated data at probability level $\xi = 0.99$. The estimated regression lines are superimposed to each scatter plot. The associated slope is an estimation of the tail-index γ. Bottom: estimated $\lambda(\cdot)$ functions. Black: original simulated data ($\gamma = 0.9$, $\rho_1 = -1$, $\rho_2 = -3$ and $\mu = 10$), blue: data generated with Tail-GAN model, orange: data generated with classic GAN model.

`polytechnique.fr/user_doc/`. It is composed by 2 nodes, where each one includes 2 CPU Intel Xeon Gold 6230 @ 2.1GHz, 20 cores and 4 Nvidia Tesla v100 graphics card. All the code was implemented in Python 3.8.2 and using the library PyTorch 1.7.1 for the GANs' training.

3.4 Results

Both GAN and Tail-GAN are trained on each of the 27 simulated datasets independently during the $1,000$ iterations with various neural network hyperparameter tunings listed in Table 1. Every 5 iterations, two metrics are computed and the best results among the 200 checkpoints are used as a model selection technique for each metric. The first one is the SSLE at level $\xi = 0.99$ and the best results are recorded on the upper panel of Table 2. The second one is the AKE criterion with all data ($\xi = 0$) and the best results are recorded on the middle panel of Table 2. The associated Kendall's tau is also reported on the bottom

panel of Table 2. Information on the selected hyperparameters on the simulated data is provided in Table 1.

When the tail-index γ increases, the tails of the marginal distributions of the simulated get heavier and the SSLE criteria of GAN and Tail-GAN methods increase for all considered values of (ρ_1, ρ_2, μ) with a clear soaring when $\gamma = 1$. In this latter case, the expectation of the simulated distribution does not exist. However, from this marginal point of view, Tail-GAN outperforms GAN in terms of SSLE for all considered configurations of $(\gamma, \rho_1, \rho_2, \mu)$. This conclusion remains true from the dependence point of view: Tail-GAN outperforms GAN in terms of AKE for all the considered configurations of (ρ_1, ρ_2, μ) when $\gamma \in \{0.5, 0.9\}$. This phenomenon is illustrated in Figure 5 in the case where $\gamma = 0.9$, $\rho_1 = -1$, $\rho_2 = -3$ and $\mu = 10$. The log quantile-quantile plots associated with both margins are displayed on the top panel. It is easily seen that GAN method is not able to generate data in the distribution tail since the tail heaviness is strongly underestimated. This common phenomenon in GAN training is called mode-collapse, which appears when both the generator and the discriminator overfit the data. This entails a very small diversification of the generator's outputs. At the opposite, Tail-GAN method yields realistic data generation in both marginal tail distributions. Note that, in this case, the dependence structure is well captured by both neural networks, see the estimated $\lambda(\cdot)$ functions on the bottom panel.

Finally, it appears on Table 2 that Kendall's tau is not a sufficient summary of the dependence structure: All estimated Kendall's tau are close to the theoretical ones even though the AKE is large. This criterion is thus dropped in the real data analysis hereafter since it might lead to misleading conclusions.

4. Illustration on real financial data

Our approach is tested on closing prices of daily financial indices taken from `https://stooq.com/db/h/` on the 10/01/2020. This database includes 61 world indices from their first day of quotation. Here, we selected 6 indices: NKX (Nikkei, Japan), KOSPI (Korea), HSI (Hong-Kong), CAC (France), AMX (Amsterdam Exchange, Netherlands), Nasdaq (USA) from 3 market zones: Asia, Europe, USA.

As a pre-processing step, the daily log-returns are computed for each ticker index. In case of missing data at a given business day, the next available day is removed from the dataset. Also, since we are interested in the modeling of synchronous indices, we kept only the data available at the same date for all selected 6 tickers. Finally, positive returns were discarded since we focus on the generation of losses.

Figure 6 proposes a graphical summary of the tail and dependence properties associated with this dataset. First, the log quantile-quantile plots computed on all indices at level $\xi = 0.95$ are approximately linear which provides a graphical evidence of the tail heaviness of all six marginal distributions, with estimated slopes pointing towards a tail-index $\gamma \simeq 0.3$. Second, the $\lambda(\cdot)$ associated with all 15 pairs of indices are also displayed together with the two extreme cases $\lambda_\Pi(\cdot)$ and $\lambda_M(\cdot)$. The strongest dependence is found within the European market zone (pair AMX,CAC) while weakest dependences are located between US and Asian market zones. Let us however note that the dependence between Asian, European and US markets may be under-estimated due to different time zones.

In the following, the performance of GAN and Tail-GAN approaches are compared on four datasets of increasing dimensions: NKX, Europe (AEX, CAC), Asia (NKX, KOSPI, HSI) and world (AEX, CAC, NKX, KOSPI, HSI, NDQ). The training procedure described in Section 3 is adopted and results are reported in Table 3. Tail-GAN outperforms GAN both on tail criteria SSLE(ξ), $\xi \in \{0.90, 0.95, 0.99\}$ and on dependence criterion AKE. These results are illustrated on Figure 7 where it appears that Tail-GAN is able to generate financial indices with realistic marginal tail behaviors. Finally, Figure 8 provides a comparison of dependence results obtained either using the SSLE or the AKE criteria. Unsurprisingly, the latter yields better results. Here again, the results associated with Tail-GAN are visually more satisfying than those of the classic GAN. Information on the selected hyperparameters on the real data is provided in Table 1.

ticker	NKX		Europe		Asia		World	
dimension d	1		2		3		6	
sample size n	3173		2504		1378		548	
SSLE(0.90)	1.500	**0.421**	9.651	**0.330**	3.223	**0.927**	1.785	**0.472**
SSLE(0.95)	1.173	**0.163**	6.156	**0.222**	1.007	**0.394**	1.206	**0.329**
SSLE(0.99)	0.428	**0.062**	0.698	**0.080**	0.133	**0.070**	0.250	**0.098**
AKE	–	–	16.807	**4.697**	9.760	**4.872**	24.781	**3.533**

Table 3: Performance comparaison between the best GAN and the Tail-GAN (in bold) results on real data using the SSLE(ξ) criteria computed at levels $\xi \in \{0.90, 0.95, 0.99\}$ and the AKE criterion (results are multiplied by 10^3 for the sake of readability).

5. Conclusion

In this work, we have introduced a new generative method called Tail-GAN dedicated to extreme events. It relies on a new parametrization of GANs allowing to generate data coming from a heavy-tailed distribution. From the theoretical point of view, the uniform convergence rate of the proposed transformed quantile function f^{TIF} by a one hidden-layer ReLU neural network is established within an extreme-value framework. From the practical point of view, we have illustrated on real and simulated data that Tail-GAN outperforms classic GAN both in terms of tail behavior of the marginal distributions and in terms of dependence structure.

To complete the current theoretical analysis which ensures accurate approximation of marginals using NN, our further work will be dedicated to investigate mathematically how dependence structure is preserved, leveraging multivariate extreme-value theory. The analysis goes far beyond this work since it is known that dependence structure in the tails can be quite different from one case to another (Coles et al., 1999).
Finally, we shall investigate the behaviour of the proposed Tail-GAN corrections in other GAN architectures, using different distances and alternative criteria to LSSE and AKE.

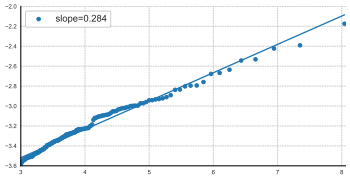

(a) AEX

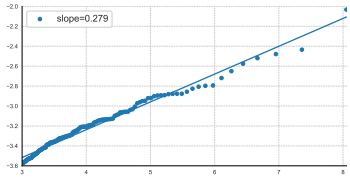

(b) CAC

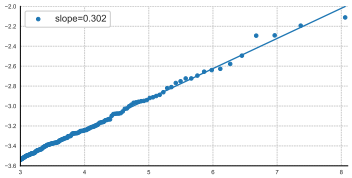

(c) NKX

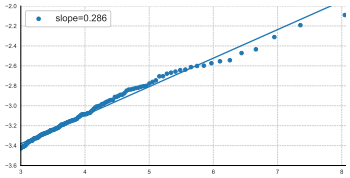

(d) KOSPI

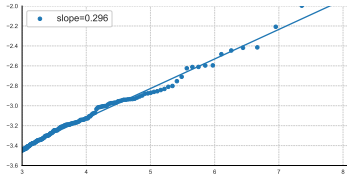

(e) HSI

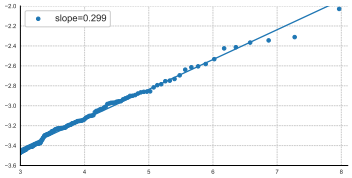

(f) NDQ

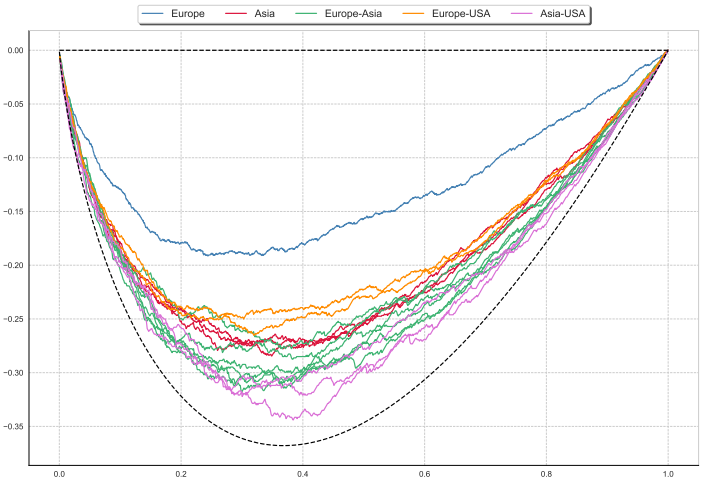

(g) Estimated $\lambda(\cdot)$ functions

Figure 6: Top panels: Log quantile-quantile plots on the 6 selected financial indices at probability level $\xi = 0.95$. The estimated regression line is superimposed to each scatter plot. The associated slope is an estimation of the tail-index. Bottom panel: Estimated $\lambda(\cdot)$ functions for all 15 pairs of indices. Functions $\lambda_\Pi(t) = t \log t$ and $\lambda_M(t) = 0$ respectively associated to independence and comotonic dependence in the bivariate case ($d = 2$) are depicted by black dashed lines.

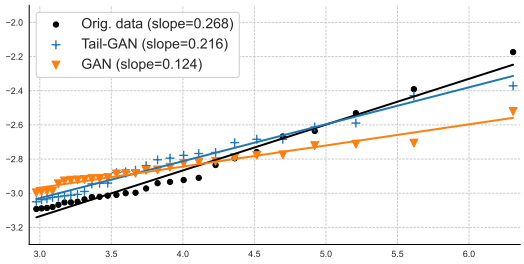

(a) AEX

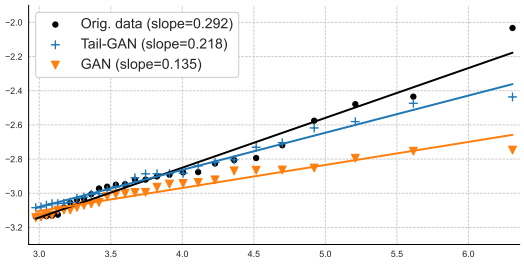

(b) CAC

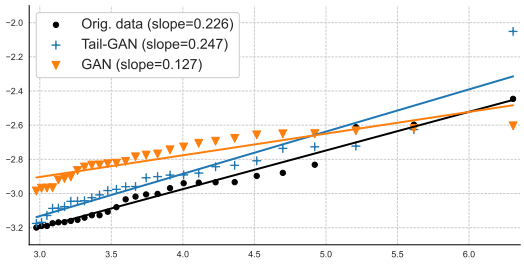

(c) NKX

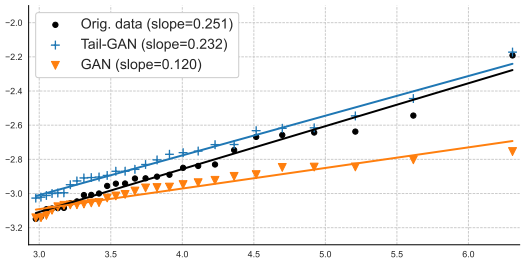

(d) KOSPI

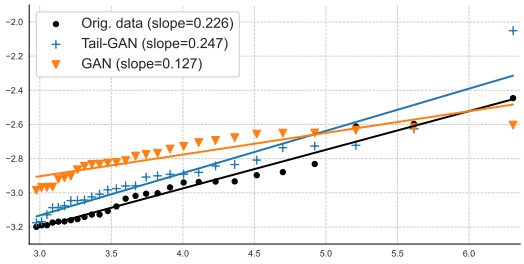

(e) HSI

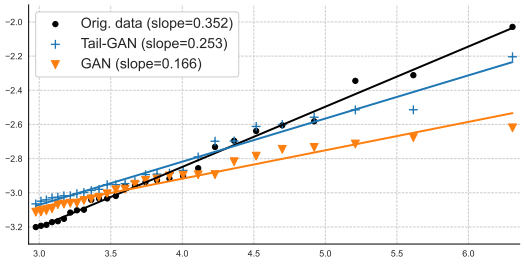

(f) NDQ

Figure 7: Log quantile-quantile plots associated with the world market zone at probability level $\xi = 0.95$.

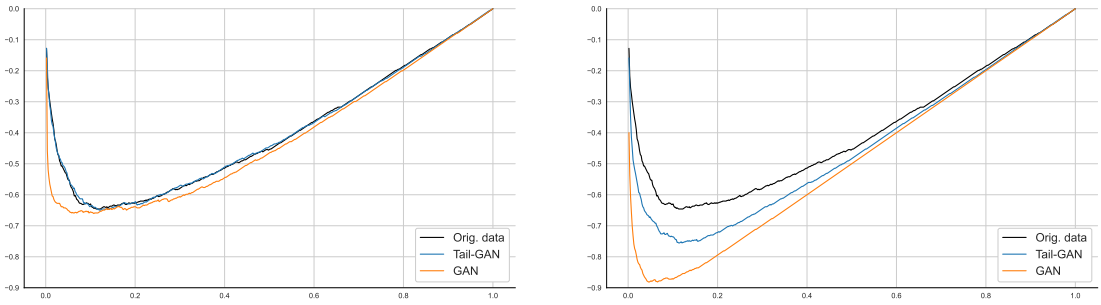

(a) (b)

Figure 8: Estimated $\lambda(\cdot)$ functions associated with the World market zone ($d = 6$). Black: original real data, blue: data generated with Tail-GAN model, orange: data generated with classic GAN model. (a) AKE criterion, (b) SSLE(0.95) criterion.

Distribution (parameters)	Density function	γ	ρ
Pareto ($\alpha > 0$)	$\alpha t^{-\alpha-1}$ $(t > 1)$	$1/\alpha$	$-\infty$
Burr ($\alpha, \beta > 0$)	$\alpha\beta t^{\alpha-1}\left(1+t^{\alpha}\right)^{-\beta-1}$ $(t > 0)$	$1/(\alpha\beta)$	$-1/\beta$
Fréchet ($\alpha > 0$)	$\alpha t^{-\alpha-1}\exp\left(-t^{-\alpha}\right)$ $(t > 0)$	$1/\alpha$	-1
Fisher ($\nu_1, \nu_2 > 0$)	$\frac{(\nu_1/\nu_2)^{\nu_1/2}}{B(\nu_1/2,\nu_2/2)} t^{\nu_1/2-1}(1+\nu_1 t/\nu_2)^{-(\nu_1+\nu_2)/2}$ $(t > 0)$	$2/\nu_2$	$-2/\nu_2$
Inverse-Gamma ($\alpha, \beta > 0$)	$\frac{\beta^{\alpha}}{\Gamma(\alpha)} t^{-\alpha-1}\exp(-\beta/t)$ $(t > 0)$	$1/\alpha$	$-1/\alpha$
Cauchy ($\sigma > 0$)	$\frac{\sigma}{\pi(\sigma^2+t^2)}$	1	-2
Student ($\nu > 0$)	$\frac{1}{\sqrt{\nu\pi}} \frac{\Gamma\left(\frac{\nu+1}{2}\right)}{\Gamma\left(\frac{\nu}{2}\right)} \left(1+\frac{t^2}{\nu}\right)^{-\frac{\nu+1}{2}}$	$1/\nu$	$-2/\nu$

Table 4: A list of heavy-tailed distributions with the associated values of γ and ρ.

Acknowledgments

This action benefited from the support of the Chair Stress Test, Risk Management and Financial Steering, led by the French Ecole polytechnique and its foundation and sponsored by BNP Paribas. This work has been partially supported by MIAI @ Grenoble Alpes, (ANR-19-P3IA-0003).

Appendix A collects some statistical tools based on copulas used in experiments (Section 3 and Section 4). Appendix B provides auxiliary results used in Appendix C to prove the main results of Section 2.

Appendix A. Copulas

Let us consider a $d-$ variate cumulative distribution function F_X with continuous margins denoted by $F_X^{(j)}$, $j \in \{1, \dots, d\}$. From Sklar's Theorem (Sklar, 1959), there exists a unique function C such that

$$F_X\left(x^{(1)}, \dots, x^{(d)}\right) = C\left(F_X^{(1)}(x^{(1)}), \dots, F_X^{(d)}(x^{(d)})\right),$$

with $\left(x^{(1)}, \dots, x^{(d)}\right) \in \mathbb{R}^d$. The function C is called the copula of F_X. Introducing the uniform random variables $U^{(j)} = F^{(j)}(X^{(j)})$ for all $j \in \{1, \dots, d\}$, the copula C is the $d-$ dimensional distribution function of the random vector $\left(U^{(1)}, \dots, U^{(d)}\right)$ with uniform margins on $[0, 1]$. Copulas are a flexible tool to impose a given dependence structure on the marginal distributions of interest, see (Nelsen, 2006) for a detailed account on copulas. The independence between margins corresponds to the product copula $\Pi(u^{(1)}, \dots, u^{(d)}) = u^{(1)} \dots u^{(d)}$ while comotonic dependence corresponds to the Fréchet copula $M(u^{(1)}, \dots, u^{(d)}) = \min(u^{(1)}, \dots, u^{(d)})$.

Archimedean copulas. An Archimedean copula C_μ is defined for all $(u^{(1)}, \dots, u^{(d)}) \in [0, 1]^d$ by

$$C_\mu\left(u^{(1)}, \dots, u^{(d)}\right) = \psi_\mu\left(\psi_\mu^{-1}(u^{(1)}) + \dots + \psi_\mu^{-1}(u^{(d)})\right),$$

where $\psi_\mu : [0, \infty) \to [0, 1]$ is a parametric function which has to verify certain properties listed for instance in (McNeil and Nešlehová, 2009).

Kendall's dependence function. Kendall's dependence function (Genest and Rivest, 1993) characterizes the dependence structure associated with a copula C and is the univariate cumulative distribution function defined by $K_C(t) = \mathbb{P}\left(C\left(U^{(1)}, \dots, U^{(d)}\right) \leq t\right)$ for all $t \in [0, 1]$. In the case of an Archimedean copula C_μ, it can be derived as (Garcin et al., 2018):

$$K_{C_\mu}(t) = t + \sum_{j=1}^{d-1} \frac{(-\psi_\mu^{-1}(t))^j}{j!} \psi_\mu^{(j)}(\psi_\mu^{-1}(t)),$$

and we shall thus consider $\lambda_{C_\mu}(t) := t - K_{C_\mu}(t)$. It is then easily seen that, when $d = 2$, $\lambda_M(t) = 0$ and $\lambda_\Pi(t) = t \log(t)$ for all $t \in (0, 1]$.

Kendall's tau (bivariate case). Kendall's tau (Kendall, 1938) is a measure of dependence between two random variables. Let us then assume $d = 2$ and let X and $\tilde{X}$ be two bivariate random vectors from F_X. Kendall's tau is defined as the probability of concordance minus the probability of discordance of $X = (X^{(1)}, X^{(2)})$ and $\tilde{X} = (\tilde{X}^{(1)}, \tilde{X}^{(2)})$. It can be shown (Nelsen, 2006, Theorem 5.1.3) that this quantity only depends on the copula C of F_X and is given by

$$\tau_C = 4\mathbb{E}\left[C(U^{(1)}, U^{(2)})\right] - 1 = 4\int_0^1 \int_0^1 C(u,v)\,\mathrm{d}C(u,v) - 1,$$

with $\tau_M = 1$ and $\tau_\Pi = 0$ as special cases. In case of an Archimedean copula C_μ, Kendall's tau and Kendall's dependence functions are linked (Genest and MacKay, 1986):

$$\tau_{C_\mu} = 1 + 4\int_0^1 \lambda_{C_\mu}(v)\,\mathrm{d}v,$$

meaning that τ_{C_μ} can be interpreted as a summary of the dependence information encoded in $\lambda_{C_\mu}(\cdot)$.

Sampling (bivariate case). Sampling a random pair (U, V) from a bivariate copula C can be achieved by first simulating $(U, W) \sim \mathcal{U}([0,1]^2)$ and then letting $V = C_u^{-1}(W)$ where C_u is the conditional copula defined by

$$C_u(v) = \mathbb{P}(V \leq v | U = u) = \partial_u C(u, v).$$

In the case of bivariate Archimedean copulas, the conditional copula and its inverse are given by (Bernard and Czado, 2015):

$$C_{\mu,u}(v) = \frac{\psi_\mu^{-1}(u)}{\partial_u \psi_\mu(C(u,v))},$$
$$C_{\mu,u}^{-1}(y) = \psi_\mu^{-1}\left(\psi_\mu\left((\partial_u\psi_\mu)^{-1}\left(\frac{\partial_u\psi_\mu(u)}{y}\right)\right) - \psi_\mu(u)\right).$$

We also refer to Wu et al. (2007) and Hofert (2008) for alternative methods based on Kendall's dependence function and Laplace transform respectively.

Inference. The estimation of Kendall's dependence function is based on the pseudo-observations $\{Z_1, \ldots, Z_n\}$ from the cumulative distribution function K and computed as

$$Z_i = \frac{1}{n-1}\sum_{j \neq i}^{n} \mathbb{1}\left\{X_j^{(1)} < X_i^{(1)}, \ldots, X_j^{(d)} < X_i^{(d)}\right\}, \tag{19}$$

for all $i \in \{1, \ldots, n\}$, see (Genest and Rivest, 1993). The estimator of K is computed using the associated empirical cumulative distribution function:

$$\hat{K}_n(t) = \frac{1}{n}\sum_{i=1}^{n} \mathbb{1}\left\{Z_i \leq t\right\},$$

and we set $\hat{\lambda}_n(t) = t - \hat{K}_n(t)$, for all $t \in [0,1]$. Similarly, Kendall's tau is estimated by

$$\hat{\tau}_n = \frac{4}{n}\sum_{i=1}^{n} Z_i - 1.$$

Appendix B. Auxiliary results

We begin with a constructive proof of a particular case of Kuratowski Theorem (Bertsekas and Shreve, 1978, Chapter 7)-(Villani, 2009, p.8).

Lemma 7 *Let X be a random variable on $\mathbb{R}^d$. There exists a mesurable function $G : (0,1) \to \mathbb{R}^d$ such that $X \overset{\mathrm{d}}{=} G(U)$ with $U \sim \mathcal{U}([0,1])$.*

Proof Let $C : \mathbb{R}^d \to (0,1)^d$ be the component-wise logistic bijective function defined as $C^{(m)}(x) = 1/(1+\exp(-x^{(m)}))$ for all $m \in \{1,\dots,d\}$. Let us also consider the continuous bijection $S : [0,1] \to [0,1]^d$ associated with the Space filling curve (Peano, 1890; Hilbert, 1891). Then, $k := S^{-1} \circ C$ is a continuous bijection from $\mathbb{R}^d$ to $(0,1)$. Additionally, let $Y := k(X)$ be a random variable on $(0,1)$ with cumulative distribution function F_Y so that $F_Y^{-1}(U) \overset{\mathrm{d}}{=} Y$, set $G(u) = k^{-1}\left(F_Y^{-1}(u)\right)$, for all $u \in (0,1)$. Then, for any bounded test function $\varphi : (0,1) \to \mathbb{R}^d$ we get

$$\mathbb{E}\left[\varphi(G(U))\right] = \mathbb{E}\left[\varphi\left(k^{-1}\left(F_Y^{-1}(U)\right)\right)\right] = \mathbb{E}\left[\varphi\left(k^{-1}(Y)\right)\right] = \mathbb{E}\left[\varphi(X)\right],$$

which proves that $X \overset{\mathrm{d}}{=} G(U)$. ■

The following three lemmas provide asymptotic expansions that will reveal useful to establish the behavior of the TIF function as well as its derivatives in the neighbourhood of $u = 0$ and $u = 1$.

Lemma 8

(i) The following asymptotic expansions hold, as $u \to 1$:

$$\frac{1}{\log\left(\frac{1-u^2}{2}\right)} = \frac{1}{\log(1-u)} + \frac{1-u}{2\left(\log(1-u)\right)^2} + \mathcal{O}\left(\frac{(1-u)^2}{\left(\log(1-u)\right)^2}\right), \tag{20}$$

$$\begin{aligned}\partial_u\left[\frac{1}{\log\left(\frac{1-u^2}{2}\right)}\right] &= \frac{1}{(1-u)\left(\log(1-u)\right)^2} - \frac{1}{2\left(\log(1-u)\right)^2} + \frac{1}{\left(\log(1-u)\right)^3} \\ &\quad + \mathcal{O}\left(\frac{(1-u)}{\left(\log(1-u)\right)^2}\right),\end{aligned} \tag{21}$$

$$\begin{aligned}\partial_{uu}^2\left[\frac{1}{\log\left(\frac{1-u^2}{2}\right)}\right] &= \frac{1}{(1-u)^2\left(\log(1-u)\right)^2} + \frac{2}{(1-u)^2\left(\log(1-u)\right)^3} \\ &\quad - \frac{1}{(1-u)\left(\log(1-u)\right)^3} + \frac{3}{(1-u)\left(\log(1-u)\right)^4} \\ &\quad + \frac{1}{4\left(\log(1-u)\right)^2} + \mathcal{O}\left(\frac{1}{\left(\log(1-u)\right)^3}\right).\end{aligned} \tag{22}$$

(ii) Assume $(\mathbf{H_1})$ and $(\mathbf{H_2})$ hold. Then,

$$q_Y(u) = \eta^{-\gamma}(1-u)^{-\gamma} L\left(\frac{1}{(1-u)\eta}\right), \tag{23}$$

$$\partial_u q_Y(u) = \eta^{-\gamma}(1-u)^{-(\gamma+1)} L\left(\frac{1}{(1-u)\eta}\right)\left(\gamma + \varepsilon\left(\frac{1}{(1-u)\eta}\right)\right), \tag{24}$$

$$\log q_Y(u) = -\gamma\log(1-u) - \beta + \frac{1}{\rho}\varepsilon\left(\frac{1}{(1-u)\eta}\right)\big(1+o(1)\big), \ \text{as } u\to 1, \tag{25}$$

$$\partial_u \log q_Y(u) = (1-u)^{-1}\left(\gamma + \varepsilon\left(\frac{1}{(1-u)\eta}\right)\right). \tag{26}$$

(iii) Assume $(\mathbf{H_1})$, $(\mathbf{H_2})$ *and* $(\mathbf{H_3})$ *hold. Then, as* $u\to 1$,

$$\partial^2_{uu} q_Y(u) = \eta^{-\gamma}(1-u)^{-(\gamma+2)} L\left(\frac{1}{(1-u)\eta}\right) \times\left[\gamma^2+\gamma+(1+2\gamma+\rho+o(1))\varepsilon\left(\frac{1}{(1-u)\eta}\right)\right], \tag{27}$$

$$\partial^2_{uu}\log q_Y(u) = (1-u)^{-2}\left(\gamma+\varepsilon\left(\frac{1}{(1-u)\eta}\right)(1+\rho+o(1))\right). \tag{28}$$

Proof *(i)* The proof of (20)–(22) is straightforward but requires tedious calculations which can be checked by a formal calculation software (using `sympy` in `Python` for instance, see below). Details are omitted here.

```
import sympy as spy
u = spy.symbols('u')

f = 1 / spy.log((1 - u ** 2) / 2)

# series as u->1
f.series(u, 1, 2, dir="-")

f_first = spy.diff(f, u)
f_first.series(u, 1, 1, dir="-")

f_second = spy.diff(f_first, u)
f_second.series(u, 1, 1, dir="-")
```

(ii) Under $(\mathbf{H_1})$, Equations (7), (8) and (10) entail

$$q_Y(u) = \eta^{-\gamma}(1-u)^{-\gamma} L\left(\frac{1}{(1-u)\eta}\right),$$

which proves (23) and moreover, owing to $(\mathbf{H_2})$,

$$\log q_Y(u) = -\gamma\log(1-u) + \log(c_\infty) - \gamma\log\eta + \int_1^{\frac{1}{(1-u)\eta}} \frac{\varepsilon(t)}{t}\,\mathrm{d}t. \tag{29}$$

By differentiating, we get

$$\partial_u q_Y(u) = q_Y(u)\times\partial_u(\log q_Y(u)) = \eta^{-\gamma}(1-u)^{-(\gamma+1)} L\left(\frac{1}{(1-u)\eta}\right)\left(\gamma+\varepsilon\left(\frac{1}{(1-u)\eta}\right)\right),$$

and (24) is proved. Now, $t \mapsto \varepsilon(t)/t$ is regularly varying with index $\rho - 1 < -1$ and thus, $\int_1^\infty \varepsilon(t)/t \, \mathrm{d}t$ is finite leading to:

$$\log L_\infty = \log c_\infty + \int_1^\infty \frac{\varepsilon(t)}{t} \, \mathrm{d}t.$$

Replacing in (29) yields:

$$\log q_Y(u) = -\gamma \log(1-u) - \beta - \int_{\frac{1}{(1-u)\eta}}^\infty \frac{\varepsilon(t)}{t} \, \mathrm{d}t.$$

Moreover, Karamata's theorem (de Haan and Ferreira, 2006, Equation (B.1.9)) states that

$$\int_x^\infty \frac{\varepsilon(t)}{t} \, \mathrm{d}t = -\frac{1}{\rho}\varepsilon(x)(1 + o(1)),$$

as $x \to \infty$ so that (25) is proved. Finally, (26) is a direct consequence of (23) and (24).

(iii) From (24), letting $U(u) = \eta^{-\gamma}(1-u)^{-(\gamma+1)} L\left(\frac{1}{(1-u)\eta}\right)$, one has

$$\partial^2_{uu} q_Y(u) = \partial_u \left[U(u) \left(\gamma + \varepsilon \left(\frac{1}{(1-u)\eta} \right) \right) \right]. \tag{30}$$

Using the form of L under $(\mathbf{H_2})$ and $x\frac{\partial_x L(x)}{L(x)} = \varepsilon(x)$, we obtain

$$\partial_u U(u) = \eta^{-\gamma}(1-u)^{-(\gamma+2)} L\left(\frac{1}{(1-u)\eta}\right) \left(\gamma + 1 + \varepsilon \left(\frac{1}{(1-u)\eta} \right) \right). \tag{31}$$

In addition, recalling that ε is differentiable under $(\mathbf{H_3})$ yields

$$\begin{aligned}
\partial_u \left[\varepsilon \left(\frac{1}{(1-u)\eta} \right) \right] &= \eta^{-\rho}(1-u)^{-(\rho+1)} \ell \left(\frac{1}{(1-u)\eta} \right) \left(\rho + \frac{1}{(1-u)\eta} \frac{\partial \ell \left(\frac{1}{(1-u)\eta} \right)}{\ell \left(\frac{1}{(1-u)\eta} \right)} \right) \\
&= \frac{1}{(1-u)} \varepsilon \left(\frac{1}{(1-u)\eta} \right) \left(\rho + \frac{1}{(1-u)\eta} \frac{\partial \ell \left(\frac{1}{(1-u)\eta} \right)}{\ell \left(\frac{1}{(1-u)\eta} \right)} \right) \qquad (32) \\
&= \frac{1}{(1-u)} \varepsilon \left(\frac{1}{(1-u)\eta} \right) (\rho + o(1)). \qquad (33)
\end{aligned}$$

Collecting (30), (31) and (33) entails

$$\begin{aligned}
\partial^2_{uu} q_Y(u) &= \eta^{-\gamma}(1-u)^{-(\gamma+2)} L\left(\frac{1}{(1-u)\eta}\right) \\
&\quad \times \left[\left(\gamma + \varepsilon \left(\frac{1}{(1-u)\eta} \right) \right)^2 + \gamma + (1 + \rho + o(1)) \varepsilon \left(\frac{1}{(1-u)\eta} \right) \right] \\
&= \eta^{-\gamma}(1-u)^{-(\gamma+2)} L\left(\frac{1}{(1-u)\eta}\right)
\end{aligned}$$

$$\times \left[\gamma^2+\gamma+(1+2\gamma+\rho+o(1))\varepsilon\left(\frac{1}{(1-u)\eta}\right)\right]$$

which proves (27). Finally, (26) and (32) entail

$$\begin{aligned}\partial^2_{uu}\log q_Y(u) &= (1-u)^{-2}\left(\gamma+\varepsilon\left(\frac{1}{(1-u)\eta}\right)\right)\\ &\quad+(1-u)^{-2}\varepsilon\left(\frac{1}{(1-u)\eta}\right)\left(\rho+\frac{1}{(1-u)\eta}\frac{\partial\ell\left(\frac{1}{(1-u)\eta}\right)}{\ell\left(\frac{1}{(1-u)\eta}\right)}\right) \qquad (34)\end{aligned}$$

and (28) is proved owing to $(\mathbf{H_3})$. ■

Lemma 9 *Let* li *be the logarithmic integral function defined for all* $u\in(0,1)$ *as*

$$\mathrm{li}(u)=\int_0^u\frac{1}{\log(t)}\,\mathrm{d}t.$$

Then, for any $p>0$, $u^p\,\mathrm{li}(1-u)\to 0$ *as* $u\to 0$.

Proof This stems from the convexity inequality $\log(1/t)\geq 1-t$ for $t\in(0,1]$. ■

Lemma 10 *For all* $u\in(0,1)$, *let* $\Phi(u)=\sum_{j=0}^3 c_j\Phi_j(u)$. *One has:*

$$\begin{aligned}\partial^2_{uu}\left[g(u)\left(\gamma+\Phi(u)\right)\right] &= -20\gamma+\frac{c_0}{(1-u)^2\left(\log(1-u)\right)^2}+\frac{2c_0}{(1-u)^2\left(\log(1-u)\right)^3}\\ &\quad+\frac{c_1}{(1-u)\left(\log(1-u)\right)^2}+\frac{2c_2}{(1-u)\left(\log(1-u)\right)^3}+\frac{3c_3}{(1-u)\left(\log(1-u)\right)^4}\\ &\quad+\mathcal{O}\left(\frac{1}{\log(1-u)}\right), \qquad \text{as } u\to 1, \qquad (35)\\ \partial^2_{uu}\left[g(u)\left(\gamma+\Phi(u)\right)\right] &\to 5\beta, \qquad \text{as } u\to 0. \qquad (36)\end{aligned}$$

Proof Differentiating Φ yields for all $u\in(0,1)$,

$$\begin{aligned}\partial_u\Phi(u) &= \sum_{j=0}^3 c_j\varphi_j(u),\\ \partial^2_{uu}\Phi(u) &= \frac{c_0}{(1-u)^2\left(\log(1-u)\right)^2}+\frac{2c_0}{(1-u)^2\left(\log(1-u)\right)^3}+\frac{c_1}{(1-u)\left(\log(1-u)\right)^2}\\ &\quad+\frac{2c_2}{(1-u)\left(\log(1-u)\right)^3}+\frac{3c_3}{(1-u)\left(\log(1-u)\right)^4}.\end{aligned}$$

Besides, for all $u\in(0,1)$,

$$\partial^2_{uu}\left[g(u)\left(\gamma+\Phi(u)\right)\right]=20u^2\left(3-4u\right)\left(\gamma+\Phi(u)\right)+40u^3\left(1-u\right)\partial_u\Phi(u)$$

$$+ u^4 (5 - 4u) \partial^2_{uu} \Phi(u). \tag{37}$$

Remarking that $\Phi(u) = \mathcal{O}(1/\log(1-u))$ and $(1-u)\partial_u \Phi(u) = \mathcal{O}\left(1/(\log(1-u))^2\right)$ as $u \to 1$ proves (35). Similarly, Lemma 9 entails that $\mathrm{li}(1-u) = \mathcal{O}(1/u)$ as $u \to 0$ and thus $\Phi(u) = c_3/(2u^2)(1+o(1))$, $\partial_u \Phi(u) = -c_3/u^3(1+o(1))$ and $\partial^2_{uu}\Phi(u) = 3c_3/u^4(1+o(1))$ as $u \to 0$. Replacing in (37) and taking the limit as $u \to 0$ gives (36). ■

The next Lemma provides a sufficient condition for a given function to belong to $\mathcal{C}^{0,\alpha}([0,1])$.

Lemma 11 *Let $g : [0,1] \to \mathbb{R}$ be a continuous function on $[0,1]$ and differentiable on $(0,1)$ such that $|\partial_u g(u)| \leq C u^{\alpha-1}$ for all $u \in (0,1)$ with $0 < \alpha \leq 1$ and $C > 0$. Then, $g \in \mathcal{C}^{0,\alpha}([0,1])$.*

Proof Let $0 \leq a < b \leq 1$, then

$$|g(b) - g(a)| \leq \int_a^b C x^{\alpha-1} \, \mathrm{d}x \leq \int_a^b C(x-a)^{\alpha-1} \, \mathrm{d}x = \frac{C}{\alpha}(b-a)^\alpha,$$

and the conclusion follows. ■

Our goal here is to study the uniform convergence rate of the approximation error of a $\mathcal{C}^{1,\alpha}([0,1])$ or $C^2([0,1])$ function f by a neural network. To this end, consider a triangular function $\widehat{\sigma} : \mathbb{R} \to [0,1]$ built using three translated ReLU functions $x \in \mathbb{R} \mapsto \sigma(x) := \max(0, x)$:

$$\widehat{\sigma}(t) := \sigma(t+1) - 2\sigma(t) + \sigma(t-1) = \begin{cases} 1, & \text{if } t = 0, \\ 1 + t, & \text{if } -1 < t < 0, \\ 1 - t, & \text{if } 0 < t < 1, \\ 0, & \text{otherwise.} \end{cases}$$

It is then possible to control the uniform error between the function f and its piecewise linear approximation based on triangular functions, depending on the regularity of f.

Lemma 12 *Let $\widehat{\sigma}$ be a triangular function and $f : [0,1] \to \mathbb{R}$. For all $M \in \mathbb{N}\backslash\{0\}$, let $\delta = 1/M$ and $t_j = j/M$ for $j = 0, \ldots, M$. If $f \in \mathcal{C}^{1,\alpha}([0,1])$ with $\alpha \in (0,1]$, then*

$$\sup_{t \in [0,1]} \left| f(t) - \sum_{j=0}^{M} f(t_j) \widehat{\sigma}\left(\frac{t - t_j}{\delta}\right) \right| \leq \frac{[\partial_t f]_\alpha}{4} M^{-\alpha-1}. \tag{38}$$

Proof Clearly,

$$\sup_{t \in [0,1]} \left| f(t) - \sum_{j=0}^{M} f(t_j) \widehat{\sigma}\left(\frac{t - t_j}{\delta}\right) \right| =: \max_{i=0,\ldots,M-1} \sup_{t \in [t_i, t_{i+1}]} |\Delta_i(t)|,$$

where

$$\Delta_i(t) := f(t) - \left(f(t_i) \left(\frac{t_{i+1} - t}{\delta}\right) + f(t_{i+1}) \left(\frac{t - t_i}{\delta}\right) \right).$$

Two first order Taylor expansions yield that there exist $t_i' \in (t_i, t)$ and $t_i'' \in (t, t_{i+1})$ such that

$$\begin{aligned}\Delta_i(t) &= f(t) - \left[\big(f(t) + \partial_t f(t_i')(t_i - t)\big)\left(\frac{t_{i+1}-t}{\delta}\right) + \big(f(t) + \partial_t f(t_i'')(t_{i+1} - t)\big)\left(\frac{t-t_i}{\delta}\right)\right] \\ &= \frac{(t_{i+1}-t)(t-t_i)}{\delta}\left(\partial_t f(t_i') - \partial_t f(t_i'')\right).\end{aligned}$$

Remarking $(t_{i+1}-t)(t-t_i)$ is maximum on $[t_i, t_{i+1}]$ at $t = (t_{i+1}+t_i)/2$ entails

$$|\Delta_i(t)| \le \frac{\delta}{4}\left|\partial_t f(t_i') - \partial_t f(t_i'')\right| \le \frac{\delta}{4}[\partial_t f]_\alpha (t_i'' - t_i')^\alpha \le \frac{1}{4}[\partial_t f]_\alpha \delta^{\alpha+1},$$

and the result is proved. ■

Finally, one can determine the minimum number $J(\varepsilon)$ of ReLU functions to approximate f with a given precision ε. The above construction in Lemma 12 involves $(M+1)$ triangular functions corresponding to $J = 3(M+1)$ ReLU functions. Fixing bound (38) to ε provides M as a function of ε, and we obtain:

Lemma 13 *Let σ be a ReLU function and $f : [0,1] \to \mathbb{R}$. For all $\varepsilon > 0$, let $J(\varepsilon) = 3(M(\varepsilon)+1)$ with $M(\varepsilon) \in \mathbb{N}$ such that*

$$M(\varepsilon) \ge \left(\frac{[\partial_t f]_\alpha}{4\varepsilon}\right)^{1/(\alpha+1)},$$

if $f \in \mathcal{C}^{1,\alpha}([0,1])$ with $\alpha \in (0,1]$. Then, there exist $(a_j, w_j, b_j) \in \mathbb{R}^3$, $j = 1, \dots, J(\varepsilon)$ such that

$$\sup_{t\in[0,1]} \left| f(t) - \sum_{j=1}^{J(\varepsilon)} a_j \sigma\left(w_j t + b_j\right)\right| \le \varepsilon.$$

Appendix C. Proof of main results

Proof of Proposition 1. The continuity of f^{TIF} on $(0,1)$ is a consequence of the assumptions on F_X. Besides, $q_X(1-\eta) = 1$ and thus

$$f^{\mathrm{TIF}}(0) = \log(q_X(1-\eta))/\log 2 = 0.$$

From $(\mathbf{H_1})$, the cumulative distribution function F_X has an unbounded right-hand support, and thus, from (8), $q_Y(u) \to \infty$ as $u \to 1$. Thus, replacing in (7) and taking the log yields

$$\log q_Y(u) = -\gamma \log\big((1-u)\eta\big)\left(1 - \frac{\log L\left(\frac{1}{(1-u)\eta}\right)}{\gamma \log\left((1-u)\eta\right)}\right).$$

Since L is slowly varying, $\log L(v)/\log v \to 0$ as $v \to \infty$ (Bingham et al., 1987, Proposition 1.3.6) and then,

$$\log q_Y(u) = -\gamma \log(1-u)(1+o(1)), \text{ as } u \to 1.$$

Similarly, as $u \to 1$, $\log\left(\frac{1-u^2}{2}\right) = \log(1-u)(1+o(1))$, which leads to $f^{\text{TIF}}(u) \to \gamma$ as $u \to 1$. Finally, f^{TIF} is bounded on $[0,1]$ and the conclusion follows. ■

Proof of Proposition 2. First, $q_Y(0) = 1$ directly yields

$$\partial_u f^{\text{TIF}}(0) = \frac{\gamma + \varepsilon\left(1/\eta\right)}{\log(2)}.$$

Second, collecting (20) and (26), it follows, as $u \to 1$,

$$\begin{aligned}\frac{\partial_u \log q_Y(u)}{\log\left(\frac{1-u^2}{2}\right)} &= \frac{\gamma}{(1-u)\log(1-u)} + \frac{\gamma}{2\left(\log(1-u)\right)^2} + \frac{\varepsilon\left(\frac{1}{(1-u)\eta}\right)}{(1-u)\log(1-u)} + \mathcal{O}\left(\frac{(1-u)}{\left(\log(1-u)\right)^2}\right) \\ &= \frac{\gamma}{(1-u)\log(1-u)} + \frac{\gamma}{2}\varphi_2(u) + \frac{\varepsilon\left(\frac{1}{(1-u)\eta}\right)}{(1-u)\log(1-u)} + \mathcal{O}\left(\frac{(1-u)}{\left(\log(1-u)\right)^2}\right).\end{aligned}$$

In addition, from (21) and (25), we have, as $u \to 1$,

$$\begin{aligned}\log q_Y(u)\partial_u\left[\frac{1}{\log\left(\frac{1-u^2}{2}\right)}\right] &= \frac{-\gamma}{(1-u)\log(1-u)} - \frac{\beta}{(1-u)\left(\log(1-u)\right)^2} + \frac{\gamma}{2\log(1-u)} \\ &\quad - \frac{(2\gamma-\beta)}{2\left(\log(1-u)\right)^2} - \frac{\beta}{\left(\log(1-u)\right)^3} + \frac{\varepsilon\left(\frac{1}{(1-u)\eta}\right)(1+o(1))}{\rho(1-u)\left(\log(1-u)\right)^2} \\ &\quad + \mathcal{O}\left(\frac{(1-u)}{\log(1-u)}\right) \\ &= \frac{-\gamma}{(1-u)\log(1-u)} - \beta\varphi_0(u) + \frac{\gamma}{2}\varphi_1(u) - \frac{(2\gamma-\beta)}{2}\varphi_2(u) + \beta\varphi_3(u) \\ &\quad + \frac{\varepsilon\left(\frac{1}{(1-u)\eta}\right)(1+o(1))}{\rho(1-u)\left(\log(1-u)\right)^2} + \mathcal{O}\left(\frac{(1-u)}{\log(1-u)}\right).\end{aligned}$$

Summing up the two above expansions and inverting the signs yield

$$\begin{aligned}\partial_u f^{\text{TIF}}(u) &= \beta\varphi_0(u) - \frac{\gamma}{2}\varphi_1(u) + \frac{\gamma-\beta}{2}\varphi_2(u) + \beta\varphi_3(u) \\ &\quad - \frac{\varepsilon\left(\frac{1}{(1-u)\eta}\right)}{(1-u)\log(1-u)}\left(1 + \frac{1}{\rho\log(1-u)}(1+o(1))\right) + \mathcal{O}\left(\frac{(1-u)}{\log(1-u)}\right),\end{aligned}$$

which proves the result. ■

Proof of Proposition 3. For all $u \in (0,1)$, let $\Phi(u) = \sum_{j=0}^{3} c_j \Phi_j(u)$.
(i) First, note that $\Phi(u) \to 0$ as $u \to 1$, $h(1) = 0$ and $g(1) = 1$. Besides, Proposition 1 shows that $f^{\text{TIF}}(u) \to \gamma$ as $u \to 1$ and therefore $f^{\text{CTIF}}(u) \to 0$ as $u \to 1$. Second, Lemma 9

entails that $\mathrm{li}(1-u) = \mathcal{O}(1/u)$ as $u \to 0$ and thus $\Phi(u) = c_3/(2u^2)(1+o(1))$. It follows that $g(u)\Phi(u) \to 0$ as $u \to 0$. Clearly, one also has $g(0) = h(0) = 0$. Besides, Proposition 1 shows that $f^{\mathrm{TIF}}(0) = 0$ and therefore $f^{\mathrm{CTIF}}(u) \to 0$ as $u \to 0$.
(ii) First, differentiating (12) and taking account of $g'(1) = h'(1) = 0$, $\Phi(u) \to 0$ as $u \to 1$ yields

$$\partial_u f^{\mathrm{CTIF}}(u) = \partial_u f^{\mathrm{TIF}}(u) - \partial_u \Phi(u) g(u) + o(1) = \partial_u \Phi(u)\,(1 - g(u)) + o(1),$$

as $u \to 1$, since $\partial_u f(u) = \partial_u \Phi(u) + o(1)$ when $\rho < -1$, in view of (11) in Proposition 2. Remarking that $1 - g(u) = o(1-u)$ and recalling from the proof of Lemma 10 that $(1-u)\partial_u \Phi(u) = \mathcal{O}\left(1/(\log(1-u))^2\right)$ as $u \to 1$ prove that $\partial_u f^{\mathrm{CTIF}}(u) \to 0$ as $u \to 1$. Second, taking account of $g'(0) = 0$ and $h'(0) = 1$ yields

$$\partial_u f^{\mathrm{CTIF}}(u) = -g(u)\partial_u \Phi(u) - \Phi(u)\partial_u g(u) + o(1),$$

as $u \to 0$. Recall from the proof of Lemma 10 that $\Phi(u) = c_3/(2u^2)(1+o(1))$ and $\partial_u \Phi(u) = -c_3/u^3(1+o(1))$ as $u \to 0$. Since $g(u) = o(u^3)$ and $\partial_u g(u) = o(u^2)$ as $u \to 0$, it follows that $\partial_u f^{\mathrm{CTIF}}(u) \to 0$ as $u \to 0$ and (14) is proved.
(iii) The first part of the proof is based on successive applications of Lemma 8. From (20) and (28), one has, as $u \to 1$:

$$\partial^2_{uu}\left[\log q_Y(u)\right] \frac{1}{\log\left(\frac{1-u^2}{2}\right)} = \frac{\gamma}{(1-u)^2 \log(1-u)} + \frac{\gamma}{2(1-u)\left(\log(1-u)\right)^2} + \frac{\varepsilon\left(\frac{1}{(1-u)\eta}\right)}{(1-u)^2\log(1-u)}(1+\rho+o(1)) + \mathcal{O}\left(\frac{1}{\left(\log(1-u)\right)^2}\right).$$

Similarly, from (21) and (26), as $u \to 1$,

$$\partial_u\left[\log q_Y(u)\right]\partial_u\left[\frac{1}{\log\left(\frac{1-u^2}{2}\right)}\right] = \frac{\gamma}{(1-u)^2\left(\log(1-u)\right)^2} - \frac{\gamma}{2(1-u)\left(\log(1-u)\right)^2} + \frac{\gamma}{(1-u)\left(\log(1-u)\right)^3} + \frac{\varepsilon\left(\frac{1}{(1-u)\eta}\right)}{(1-u)^2\left(\log(1-u)\right)^2} + \mathcal{O}\left(\frac{1}{\left(\log(1-u)\right)^2}\right),$$

and, from (22) and (25),

$$\log(q_Y(u))\partial^2_{uu}\left[\frac{1}{\log\left(\frac{1-u^2}{2}\right)}\right] = -\frac{\gamma}{(1-u)^2\log(1-u)} - \frac{2\gamma+\beta}{(1-u)^2\left(\log(1-u)\right)^2} - \frac{2\beta}{(1-u)^2\left(\log(1-u)\right)^3} + \frac{\gamma}{(1-u)\left(\log(1-u)\right)^2} - \frac{3\gamma-\beta}{(1-u)\left(\log(1-u)\right)^3} - \frac{3\beta}{(1-u)\left(\log(1-u)\right)^4}$$

$$+\frac{\varepsilon\left(\frac{1}{(1-u)\eta}\right)(1+o(1))}{\rho(1-u)^2(\log(1-u))^2}+\frac{2\varepsilon\left(\frac{1}{(1-u)\eta}\right)(1+o(1))}{\rho(1-u)^2(\log(1-u))^3}$$
$$-\frac{\gamma}{4\log(1-u)}+\mathcal{O}\left(\frac{1}{(\log(1-u))^2}\right).$$

Collecting the above three asymptotic expansions yields, as $u \to 1$,

$$\begin{aligned}\partial^2_{uu} f^{\mathrm{TIF}}(u) &= \frac{\beta}{(1-u)^2(\log(1-u))^2}+\frac{2\beta}{(1-u)^2(\log(1-u))^3}-\frac{\gamma}{2(1-u)(\log(1-u))^2}\\ &+\frac{\gamma-\beta}{(1-u)(\log(1-u))^3}+\frac{3\beta}{(1-u)(\log(1-u))^4}+\frac{\gamma}{4\log(1-u)}\\ &-\frac{(1+\rho)\varepsilon\left(\frac{1}{(1-u)\eta}\right)}{(1-u)^2\log(1-u)}(1+o(1))+\mathcal{O}\left(\frac{1}{(\log(1-u))^2}\right). \qquad (39)\end{aligned}$$

In addition, note that $h''(1) = 2$ and $\partial_u f^{\mathrm{TIF}}(0) = (\gamma + \varepsilon(1/\eta))/\log(2)$ in view of Proposition 2, so that collecting (35) in Lemma 10 with (39) proves (15). The second part of the proof consists in remarking that $\log q_Y(0) = 0$ by construction and $\partial_u \left[\frac{1}{\log\left(\frac{1-u^2}{2}\right)}\right](0) = 0$. Therefore, taking account of (34), it follows:

$$\partial^2_{uu} f^{\mathrm{TIF}}(0) = \frac{\partial^2_{uu}\left[\log\left(q_Y(u)\right)\right](0)}{\log(2)} = \frac{\gamma+\varepsilon(1/\eta)\left(1+\rho+\frac{1}{\eta}\frac{\partial\ell(1/\eta)}{\ell(1/\eta)}\right)}{\log(2)}. \qquad (40)$$

Finally, note that $h''(0) = -4$ and $\partial_u f^{\mathrm{TIF}}(0) = (\gamma+\varepsilon(1/\eta))/\log(2)$ in view of Proposition 2, so that collecting (36) in Lemma 10 with (40) proves (16).
(iv) is a direct consequence of *(iii)*. ■

Proof of Corollary 4. *(i)* When $-2 < \rho \leq -1$, Proposition 3(*iii*) implies $f^{\mathrm{CTIF}} \in C^2([0,1))$ and

$$\left|\partial^2_{uu} f^{\mathrm{CTIF}}(u)\right| \leq C(1-u)^{\alpha-1}, \quad \forall u \in (0,1),$$

for any fixed $\alpha \in (0, -\rho - 1)$. Thus, applying Lemma 11 to $\partial_u f^{\mathrm{CTIF}}$ yields $f^{\mathrm{CTIF}} \in \mathcal{C}^{1,\alpha}([0,1])$.
(ii) is a direct consequence of Proposition 3(*iv*). ■

References

J. Alm. Signs of dependence and heavy tails in non-life insurance data. *Scandinavian Actuarial Journal*, 2016(10):859–875, 2016.

M. Arjovsky, S. Chintala, and L. Bottou. Wasserstein generative adversarial networks. In D. Precup and Y. W. Teh, editors, *Proceedings of the 34th International Conference on Machine Learning*, volume 70 of *Proceedings of Machine Learning Research*, pages 214–223. PMLR, 2017.

S. Asmussen and H. Albrecher. *Ruin probabilities*. Advanced Series on Statistical Science & Applied Probability, 14. World Scientific Publishing Co. Pte. Ltd., Hackensack, NJ, second edition, 2010.

J. Beirlant, Y. Goegebeur, J. Segers, and J. Teugels. *Statistics of Extremes: Theory and Applications*. Wiley, 2004.

C. Bernard and C. Czado. Conditional quantiles and tail dependence. *Journal of Multivariate Analysis*, 138:104–126, 2015.

D. P. Bertsekas and S. E. Shreve. *Stochastic optimal control*, volume 139 of *Mathematics in Science and Engineering*. Academic Press, Inc., New York-London, 1978.

S. Bhatia, A. Jain, and B. Hooi. ExGAN: Adversarial generation of extreme samples. *arXiv preprint arXiv:2009.08454*, 2020.

G. Biau, B. Cadre, M. Sangnier, and U. Tanielian. Some theoretical properties of GANs. *The Annals of Statistics*, 48(3):1539–1566, 2020a.

G. Biau, M. Sangnier, and U. Tanielian. Some theoretical insights into Wasserstein GANs. *arXiv preprint arXiv:2006.02682*, 2020b.

N. H. Bingham, C. M. Goldie, and J. L. Teugels. *Regular variation*, volume 27 of *Encyclopedia of Mathematics and its Applications*. Cambridge University Press, Cambridge, 1987.

J. A. Bucklew. *Introduction to rare event simulation*. Springer Series in Statistics. Springer-Verlag, New York, 2004.

V. Chavez-Demoulin, P. Embrechts, and S. Sardy. Extreme-quantile tracking for financial time series. *Journal of Econometrics*, 181(1):44–52, 2014.

S. Coles, J. Heffernan, and J. Tawn. Dependence measures for extreme value analyses. *Extremes*, 2(4):339–365, 1999.

G. Cybenko. Approximation by superpositions of a sigmoidal function. *Mathematics of Control, Signals, and Systems*, 2(4):303–314, 1989.

L. de Haan and A. Ferreira. *Extreme value theory*. Springer Series in Operations Research and Financial Engineering. Springer, New York, 2006.

P. Del Moral and J. Garnier. Genealogical particle analysis of rare events. *The Annals of Applied Probability*, 15(4):2496–2534, 2005.

R. Eckhardt. Stam Ulam, John Von Neumann and the Monte-Carlo method. *Los Alamos Science*, Special Issue:131–143, 1987.

P. Embrechts, C. Klüppelberg, and T. Mikosch. *Modelling Extremal Events for Insurance and Finance*. Springer-Verlag, Berlin, 1997.

European Banking Authority. Guidelines on the revised common procedures and methodologies for the supervisory review and evaluation process (SREP) and supervisory stress testing. *Available at https://eba.europa.eu/regulation-and-policy/supervisory-review-and-evaluation-srep-and-pillar-2/guidelines-for-common-procedures-and-methodologies-for-the-supervisory-review-and-evaluation-process-srep-and-supervisory-stress-testing*, EBA/GL/2014/13, 2014.

D. Foster. *Generative deep learning: teaching machines to paint, write, compose, and play.* O'Reilly Media, 2019.

M. Garcin, D. Guegan, and B. Hassani. A novel multivariate risk measure: the Kendall VaR. Technical report, 2018. URL `https://halshs.archives-ouvertes.fr/halshs-01467857`.

L. Gardes and S. Girard. Conditional extremes from heavy-tailed distributions: An application to the estimation of extreme rainfall return levels. *Extremes*, 13(2):177–204, 2010.

L. Gardes and S. Girard. Functional kernel estimators of large conditional quantiles. *Electronic Journal of Statistics*, 6:1715–1744, 2012.

C. Genest and J. MacKay. The joy of copulas: bivariate distributions with uniform marginals. *The American Statistician*, 40(4):280–283, 1986.

C. Genest and L.-P. Rivest. A characterization of Gumbel's family of extreme value distributions. *Statistics & Probability Letters*, 8(3):207–211, 1989.

C. Genest and L.-P. Rivest. Statistical inference procedures for bivariate Archimedean copulas. *Journal of the American Statistical Association*, 88(423):1034–1043, 1993.

E. Gobet and G. Liu. Rare event simulation using reversible shaking transformations. *SIAM Journal on Scientific Computing*, 37(5):A2295–A2316, 2015.

I. Goodfellow, J. Pouget-Abadie, M. Mirza, B. Xu, D. Warde-Farley, S. Ozair, A. Courville, and Y. Bengio. Generative adversarial nets. In *Advances in neural information processing systems*, pages 2672–2680, 2014.

M. Haas and S. Richter. Statistical analysis of Wasserstein GANs with applications to time series forecasting. *arXiv preprint arXiv:2011.03074*, 2020.

D. Hilbert. Ueber die stetige Abbildung einer Line auf ein Flächenstück. *Mathematische Annalen*, 38(3):459–460, 1891.

M. Hofert. Sampling Archimedean copulas. *Computational Statistics & Data Analysis*, 52 (12):5163–5174, 2008.

M. Kendall. A new measure of rank correlation. *Biometrika*, 30(1/2):81–93, 1938.

D. Kingma and J. Ba. Adam: A method for stochastic optimization. *International Conference on Learning Representations*, 2014.

D. Kingma and M. Welling. Auto-encoding variational bayes. In *2nd International Conference on Learning Representations, ICLR 2014, Banff, AB, Canada, April 14-16, 2014, Conference Track Proceedings*, 2014.

E. Kohlbecker. Weak asymptotic properties of partitions. *Transactions of The American Mathematical Society*, 88(2):346–365, 1958.

V. E. Maiorov and R. Meir. On the near optimality of the stochastic approximation of smooth functions by neural networks. *Advances in Computational Mathematics*, 13(1): 79–103, 2000.

A. McNeil and J. Nešlehová. Multivariate Archimedean copulas, d-monotone functions and l_1-norm symmetric distributions. *The Annals of Statistics*, 37(5B):3059–3097, 2009.

R. Nelsen. *An introduction to copulas*. Springer Series in Statistics. Springer, New York, second edition, 2006.

G. Peano. Sur une courbe qui remplit toute une aire plane. *Mathematische Annalen*, 36(1): 157–160, 1890.

M. Prandini and O. Watkins. Probabilistic aircraft conflict detection. *HYBRIDGE WP3: Reachability analysis for probabilistic hybrid systems*, 2005.

C. Remlinger, J. Mikael, and R. Elie. Conditional versus adversarial Euler-based generators for time series. *arXiv preprint arXiv:2102.05313*, 2021.

S. Resnick. *Heavy-Tail Phenomena: Probabilistic and Statistical Modeling*. Springer, 2007.

P. Robert. *Stochastic networks and queues*, volume 52 of *Applications of Mathematics*. Springer-Verlag, Berlin, 2003.

M. Sklar. Fonctions de répartition à n dimensions et leurs marges. *Publications de l'Institut de Statistique de l'Université de Paris*, 8:229–231, 1959.

C. Villani. *Optimal transport*, volume 338 of *Grundlehren der Mathematischen Wissenschaften [Fundamental Principles of Mathematical Sciences]*. Springer-Verlag, Berlin, 2009.

M. Vladimirova, J. Arbel, and P. Mesejo. Bayesian neural networks become heavier-tailed with depth. In *NeurIPS 2018-Thirty-second Conference on Neural Information Processing Systems*, pages 1–7, 2018.

M. Wiese, R. Knobloch, R. Korn, and P. Kretschmer. Quant GANs: deep generation of financial time series. *Quantitative Finance*, 20(9):1419–1440, 2020.

F. Wu, E. Valdez, and M. Sherris. Simulating from exchangeable Archimedean copulas. *Communications in Statistics-Simulation and Computation*, 36(5):1019–1034, 2007.

D. Yarotsky. Error bounds for approximations with deep reLu networks. *Neural Networks*, 94:103–114, 2017.

X. Zhou, Z. Pan, G. Hu, S. Tang, and C. Zhao. Stock market prediction on high-frequency data using Generative Adversarial Nets. *Mathematical Problems in Engineering*, 2018.